Electronic Supplementary Information

The Role of Ligand Redox Non-Innocence in Ring-Opening Polymerization Reactions Catalyzed by Bis(imino)pyridine Iron Alkoxide Complexes

K. R. Delle Chiaie,[a] A. B. Biernesser,[a] M. A. Ortuño,[b] B. Dereli,[b] D. A. Iovan,[c] M. J. T. Wilding,[c] B. Li,[a] C. J. Cramer[b] and J. A. Byers[a,*]

[a] Eugene F. Merkert Chemistry Center, Department of Chemistry, Boston College, 2609 Beacon St., Chestnut Hill, Massachusetts 02467, United States

[b] Department of Chemistry, Chemical Theory Center, and Supercomputing Institute, University of Minnesota, Minneapolis, Minnesota 55455, United States

[c] Department of Chemistry and Chemical Biology, Harvard University, 12 Oxford Street, Cambridge, Massachusetts 02138, United States

*_Corresponding author_. Tel.: 617-552-6725. Email address: jeffery.byers@bc.edu

Table of Contents

Experimental Procedures

General considerations. Unless stated otherwise, all reactions were carried out in oven-dried glassware in a nitrogen-filled glove box or with standard Schlenk line techniques.[1] Solvents were used after passage through a solvent purification system under a blanket of argon and then degassed briefly by exposure to vacuum. Nuclear Magnetic Resonance (NMR) spectra were recorded at ambient temperature on spectrometers operating at 400-600 MHz for ^{1}H NMR. Resonances for paramagnetic complexes are reported as chemical shift in ppm (peak with at half height, Hz). Infrared (IR) spectra were recorded on an ATR infrared spectrometer. Magnetic moments were determined by Evans' method[2] in THF by means of a procedure published by Gibson and coworkers.[3] Gel permeation chromatography (GPC) was performed on an Agilent GPC220 in THF at 40°C with three PL gel columns (10μm) in series. Molecular weights and molecular weight distributions were determined from the signal response of the RI detector relative to polystyrene standards. EPR spectra were obtained on a Bruker EleXsys E-500 CW-EPR spectrometer. Spectra were measured as frozen toluene glasses at a microwave power of 0.6325–2 mW at 77 K, 12K, and 4K. Effective g-values were obtained from spectral simulations of $S = {}^{1}/_{2}$ systems with the program Easyspin.[4] Zero-field ^{57}Fe Mössbauer spectra were measured with a constant acceleration spectrometer (SEE Co, Minneapolis, MN) at 90K. Isomer shifts are quoted relative to Fe foil at room temperature. Data was analyzed and simulated with Igor Pro 6 software (WaveMetrics, Portland, OR) by means of Lorentzian fitting functions. Samples were prepared by freezing a solution of 20-30 mg compound in benzene. SQUID magnetometry measurements were performed on a Quantum Design MPMS3 Instrument. Samples were prepared by immobilization in eicosane. Data was fit using JulX software to get the zero-field splitting parameters.[5] Statistical molar magnetic susceptibilities were calculated using the usual spin Hamiltonian approach for up to three spins with local multiplicities up to $S = 3/2$ based on:

$$H = H_{ex} + H_{ZFS} + H_{Zee}$$ where

$$H_{ex} = -2\sum_{i=1}^{ns-1}\sum_{j=i=1}^{ns} J_{ij}\overline{S}_i \cdot \overline{S}_j$$ is the exchange Hamiltonian, and

$$H_{ZFS} = \sum_{i=1}^{ns} D_i\left[S_{z,i}^2 - {}^1/_3 S_i(S_i+1) + {}^{E_i}/_{D_i}\left(S_{x,i}^2 - S_{y,i}^2\right)\right]$$ accounts for zero-field splitting, and

$$H_{Zee} = \sum_{i=1}^{ns} g\beta\overline{S}_i \cdot \overline{B}$$ is the Zeeman interaction.

J_{ij} are the exchange *coupling constants* of spins i and j, ns is the number of spins (max. four), D_i, E/D_i and g_i are the local axial and rhombic zero field splitting parameters and g-values (isotropic average)

The monomer (*rac*)-lactide was recrystallized from ethyl acetate followed by recrystallization from toluene and dried *in vacuo* prior to polymerization. The monomers ε-caprolactone, δ-valerolactone, β-butryolactone, and γ-valerolactone were dried over CaH_2 and distilled prior to polymerization. Trimethylene carbonate and ethylene carbonate were dried *in vacuo* prior to polymerization. Complexes **1** and **2** were synthesized as described previously.[6]

*Synthesis of Complex **3a**.* In a glove box, a solution of 4-methoxyphenol (0.0249 g, 0.201 mmol) in diethyl ether (10 ml) was cooled to -40 °C and added to a solution of **4** (0.100 g, 0.196 mmol) in diethyl ether (5ml) that had also been cooled to -40 °C. The reaction was allowed to stir at room temperature for one hour, and the red mixture was filtered through celite. The solvent was removed from the filtrate to yield a dark red solid (0.103 g, 96%). ^{1}H NMR (C_6D_6, broad singlets): 90.3(122.5) *m-py*, 16.5(128.7), -3.9(138.7) *m-aryl*, -12.9(231.4) *p-aryl*, -24.6(146.3), -63.9(1854.6) CC*H*$_3$ ppm. IR(neat): 3021, 2914, 2852, 1646, 1592, 1494, 1466, 1437, 1373, 1327, 1250, 1207, 1174, 1109, 1089, 1035, 958, 858, 816, 758, 690, 648, 560, 495 cm^{-1}. EA Found: C, 69.14; H, 6.43; N, 8.38. Calc. for $C_{32}H_{34}FeN_3O_2$: C, 70.07; H, 6.25; N, 7.66%

*Synthesis of Complex **3b***. In a glove box, a solution of neopentyl alcohol (0.0220 g, 0.250 mmol) in diethyl ether (2 ml) was cooled to -40 °C and added to a solution of **4** (0.130 g, 0.254 mmol) in diethyl ether (6 ml) that had also been cooled to -40°C. The reaction was allowed to stir at room temperature for 30 minutes, and then solvent was removed *in vacuo*. The resulting

residue was lyophilized in frozen benzene. The resulting powder was then dissolved in *n*-pentane and filtered through celite, and the solvent was removed from the filtrate to yield a dark red solid (0.105 g, 82%). Crystallization in *n*-pentane at -40 °C afforded crystals suitable for X-ray analysis. ^{1}H NMR (C_6D_6, broad singlets): 67.5(109.6) *m-py*, 50.6(235.5), -10.0(51.8) *m-aryl*, -15.9(45.7) *p-aryl*, -50.0(232.4) CC*H*$_3$ ppm. IR(neat): 2941, 2856, 1646, 1592, 1467, 1437, 1371, 1327, 1249, 1208, 1170, 1087, 1018, 956, 856, 814, 759, 691, 559, 494 cm^{-1}.

*General procedure for the polymerization of (rac)-lactide catalyzed by aryloxide complexes **1a** and **3a***. At room temperature in a glove box, iron aryloxide complex **1a** or **3a** (0.007 mmol) in chlorobenzene (0.9 mL) was added to a seven mL vial containing (*rac*)-lactide (0.050 g, 0.35 mmol) in chlorobenzene (0.5 mL). Aliquots were removed periodically from the reaction mixture and terminated by exposing them to air. Solvent was removed *in vacuo* and conversion was determined by ^{1}H NMR in $CDCl_3$ by integrating the methine peak of the remaining lactide versus the methine peak of poly(lactic acid). The aliquots were also analyzed by GPC to determine molecular weight and molecular weight distribution of the polymers.

*General procedure for the polymerization of ε-caprolactone catalyzed by aryloxide complexes **1a** and **3a**.* At room temperature in a glove box, iron aryloxide complex **1a** or **3a** (0.014 mmol) in toluene (1.8 mL) was added to a seven mL vial containing ε-caprolactone (0.080 g, 0.70 mmol) in toluene (1.0 mL). Aliquots were removed periodically from the reaction mixture and terminated by exposing them to air. Solvent was removed *in vacuo* and conversion was determined by ^{1}H NMR in $CDCl_3$ by integrating the α-methylene peak of the remaining ε-caprolactone versus the α-methylene peak of poly(caprolactone). The aliquots were also analyzed by GPC to determine molecular weight and molecular weight distribution of the polymers.

*General procedure for the polymerization of (rac)-lactide catalyzed by neopentoxide complexes **1b** and **3b***. At room temperature in a glove box, the desired amount of iron neopentoxide complex **1b** or **3b** in toluene (1.0 mL) was added to a seven mL vial containing (*rac*)-lactide (0.10 g, 0.7 mmol) in toluene (1.0 mL). Aliquots were removed periodically from the reaction mixture and terminated by exposing them to air. Solvent was removed *in vacuo* and conversion was determined by ^{1}H NMR in $CDCl_3$ by integrating the methine peak of the

remaining lactide versus the methine peak of poly(lactic acid). The aliquots were also analyzed by GPC to determine molecular weight and molecular weight distribution of the polymers.

*General procedure for the polymerization of ε-caprolactone with neopentoxide complexes **1b** and **3b***. Most polymerization reactions were performed at [caprolactone] = 0.34 M: At room temperature in a glove box, the desired amount of iron neopentoxide complex **1b** or **3b** in toluene (1.0 mL) was added to a seven mL vial containing ε-caprolactone (0.080 g, 0.70 mmol) in toluene (1.0 mL). Aliquots were removed periodically from the reaction mixture and terminated by exposing them to air. Solvent was removed *in vacuo* and conversion was determined by ^{1}H NMR in $CDCl_3$ by integrating the α-methylene peak of the remaining ε-caprolactone versus the α-methylene peak of poly(caprolactone). The aliquots were also analyzed by GPC to determine molecular weight and molecular weight distribution of the polymers. Reactions performed at higher concentrations were carried out by increasing the amount of ε-caprolactone added and reactions performed at lower concentrations were performed by increasing the amount of toluene added.

*General procedure for the polymerization of δ-valerolactone with neopentoxide complexes **1b** and **3b***. At room temperature in a glove box, the desired amount of iron neopentoxide complex **1b** or **3b** in toluene (1.0 mL) was added to a seven mL vial containing δ-valerolactone (0.070 g, 0.70 mmol) in toluene (1.0 mL). Aliquots were removed periodically from the reaction mixture and terminated by exposing them to air. Solvent was removed *in vacuo* and conversion was determined by ^{1}H NMR in $CDCl_3$ by integrating the α-methylene peak of the remaining δ-valerolactone versus the α-methylene peak of poly(valerolactone). The aliquots were also analyzed by GPC to determine molecular weight and molecular weight distribution of the polymers.

*General procedure for the polymerization of β-butyrolactone with neopentoxide complexes **1b** and **3b***. At room temperature in a glove box, the desired amount of iron neopentoxide complex **1b** or **3b** in toluene (1.0 mL) was added to a seven mL vial containing β-butyrolactone (0.070 g, 0.70 mmol) in toluene (1.0 mL). Aliquots were removed periodically from the reaction mixture and terminated by exposing them to air. Solvent was removed *in vacuo* and conversion was determined by ^{1}H NMR in $CDCl_3$ by integrating the α-methylene peak of the remaining β-butyrolactone versus the α-methylene peak of poly(butyrolactone). The aliquots

were also analyzed by GPC to determine molecular weight and molecular weight distribution of the polymers.

*Attempted polymerization of γ-butyrolactone with neopentoxide complexes **1b** and **3b***. At room temperature in a glove box, the desired amount of iron neopentoxide complex **1b** or **3b** (0.007 mmol) in THF (0.9 mL) was added to a seven mL vial containing γ-butyrolactone (0.070 g, 0.70 mmol) in THF (1.0 mL). The reaction was allowed to stir 24 hours at room temperature. No conversion was observed by ^{1}H NMR.

*Polymerization of trimethylene carbonate with neopentoxide complex **3b***. At room temperature in a glove box, the desired amount of iron neopentoxide complex **3b** in toluene (0.5 mL) was added to a seven mL vial containing trimethylene carbonate (0.036g, 0.35 mmol) in toluene (0.5 mL). A gel-like precipitate formed immediately. The reaction mixture was allowed to stir for 10 minutes and was quenched by exposing it to air. Solvent was removed *in vacuo* and conversion was determined by ^{1}H NMR in $CDCl_3$ by integrating the α-methylene peak of the remaining β-butyrolactone versus the α-methylene peak of poly(butyrolactone). The aliquots were also analyzed by GPC to determine molecular weight and molecular weight distribution of the polymers.

*Attempted polymerization of ethylene carbonate with neopentoxide complexes **1b** and **3b***. At room temperature in a glove box, the desired amount of iron neopentoxide complex **1b** or **3b** in THF (0.9 mL) was added to a seven mL vial containing ethylene carbonate (0.032 g, 0.36 mmol) in toluene (0.5 mL). The reaction mixture was allowed to stir at room temperature for 24 hours. No conversion was observed by ^{1}H NMR.

Attempted copolymerization of lactide and ε-caprolactone in one reaction pot. At room temperature in a glove box, the desired amount of complex **3b** in toluene (1.0 mL) was added to a seven mL vial containing (*rac*)-lactide (0.10 g, 0.70mmol) and ε-caprolactone (0.080g, 0.70mmol) in toluene (1.0 mL). Aliquots were removed periodically from the reaction mixture and terminated by exposing them to air. Solvent was removed *in vacuo* and conversion of lactide was determined by ^{1}H NMR in $CDCl_3$ by integrating the methine peak of the remaining lactide versus the methine peak of poly(lactic acid). No conversion of ε-caprolactone was observed by ^{1}H NMR. The aliquots were also analyzed by GPC to determine molecular weight and molecular weight distribution of the polymers.

Attempted copolymerization of lactide and ε-caprolactone by sequential lactide-caprolactone addition. At room temperature in a glove box, iron alkoxide complex **3b** (350 μL of a 0.0040 M solution in toluene, 0.0014 mmol) was added to a seven mL vial containing (*rac*)-lactide (0.10 g, 0.70 mmol) in toluene (2.0 mL). The reaction was allowed to stir at room temperature for six hours, and then ε-caprolactone (0.080 g, 0.70 mmol) was added. Aliquots were removed periodically from the reaction mixture and terminated by exposing them to air. Solvent was removed *in vacuo* and conversion of lactide was determined by ^{1}H NMR in $CDCl_3$ by integrating the methine peak of the remaining lactide versus the methine peak of poly(lactic acid). No conversion of ε-caprolactone was observed by ^{1}H NMR. The aliquots were also analyzed by GPC to determine molecular weight and molecular weight distribution of the polymers.

Block copolymerization of lactide and ε-caprolactone by sequential caprolactone-lactide addition. At room temperature in a glove box, complex **3b** (350 μL of a 0.0040 M solution in toluene, 0.0014 mmol) was added to a seven mL vial containing ε-caprolactone (0.080 g, 0.7 mmol) in toluene (2.0 mL). The reaction was allowed to stir at room temperature for 20 minutes, and then (*rac*)-lactide (0.10 g, 0.70 mmol) was added. Aliquots were removed periodically from the reaction mixture and terminated by exposing them to air. Solvent was removed *in vacuo* and conversion of lactide was determined by ^{1}H NMR in $CDCl_3$ by integrating the methine peak of the remaining lactide versus the methine peak of poly(lactic acid). Conversion of ε-caprolactone was determined by ^{1}H NMR in $CDCl_3$ by integrating the α-methylene peak of the remaining ε-caprolactone versus the α-methylene peak of poly(caprolactone). The aliquots were also analyzed by GPC to determine molecular weight and molecular weight distribution of the polymers.

Attempted copolymerization of lactide and δ-valerolactone in one reaction pot. At room temperature in a glove box, the desired amount of iron alkoxide complex complex **3b** (350μL of a 0.0040 M solution in toluene, 0.0014 mmol) was added to a seven mL vial containing (*rac*)-lactide (0.10 g, 0.70 mmol) and δ-valerolactone (0.080 g, 0.70 mmol) in toluene (2.0 mL). Aliquots were removed periodically from the reaction mixture and terminated by exposing them to air. Solvent was removed *in vacuo* and conversion of lactide was determined by ^{1}H NMR in $CDCl_3$ by integrating the methine peak of the remaining lactide versus the methine peak of poly(lactic acid). No conversion of δ-valerolactone was observed by ^{1}H NMR. The aliquots were

also analyzed by GPC to determine molecular weight and molecular weight distribution of the polymers.

Copolymerization of ε-caprolactone and δ-valerolactone in one reaction pot. At room temperature in a glove box, the desired amount of iron alkoxide complex **3b** (350μL of a 0.0040 M solution in toluene, 0.0014 mmol) was added to a seven mL vial containing ε-caprolactone (0.080 g, 0.70 mmol) and δ-valerolactone (0.080 g, 0.70 mmol) in toluene (2.0 mL). Aliquots were removed periodically from the reaction mixture and terminated by exposing them to air. Solvent was removed *in vacuo* and conversions of both monomers were determined by ^{1}H NMR in $CDCl_3$ by integrating the α-methylene peak of the remaining lactone monomer versus the α-methylene peak of poly(lactone). The aliquots were also analyzed by GPC to determine molecular weight and molecular weight distribution of the polymers.

Table S1. Polymerization of lactide (L) with **1a** and **3a** in chlorobenzene.[a]

Entry	Cat.	Cat. Loading (mol %)	[L] (M)	Time (min.)	Conv. (%)	M_n (kg/mol)	M_w/M_n	M_n theor.[b]	M_n expt./ M_n theor.
1	**3a**	2	0.25	20	86	16.0	1.14	6.2	2.6
2	**3a**	1	0.43	20	86	25.7	1.16	12.4	2.1
3	**3a**	0.5	0.86	20	66	32.2	1.14	19.0	1.7
4	**1a**	2	0.25	20	94	16.1	1.15	6.8	2.4

[a]Reactions were performed in PhCl at room temperature.
[b](Lactide molecular weight)([Fe]:[Lactide])(Conversion).

Table S2. Polymerization of ε-caprolactone with complexes **1a**, **1b**, and **3a**.[a]

Entry	Cat.	Temp. (°C)	Time (h)	Conv. (%)	M_n (kg/mol)	M_w/M_n
1	**1a**	24	24	0	--	--
2	**1a**	70	18	99	22.6	2.14
3	**3a**	24	24	80	30.6	2.22
4	**3a**	70	2	99	12.0	6.01
5[b]	**1b**	24	3	100	251.1	1.18

[a]Reactions performed with 2 mol% [Fe] in toluene (0.24M).
[b]Reaction performed with 0.05% [Fe] in toluene (0.24M).

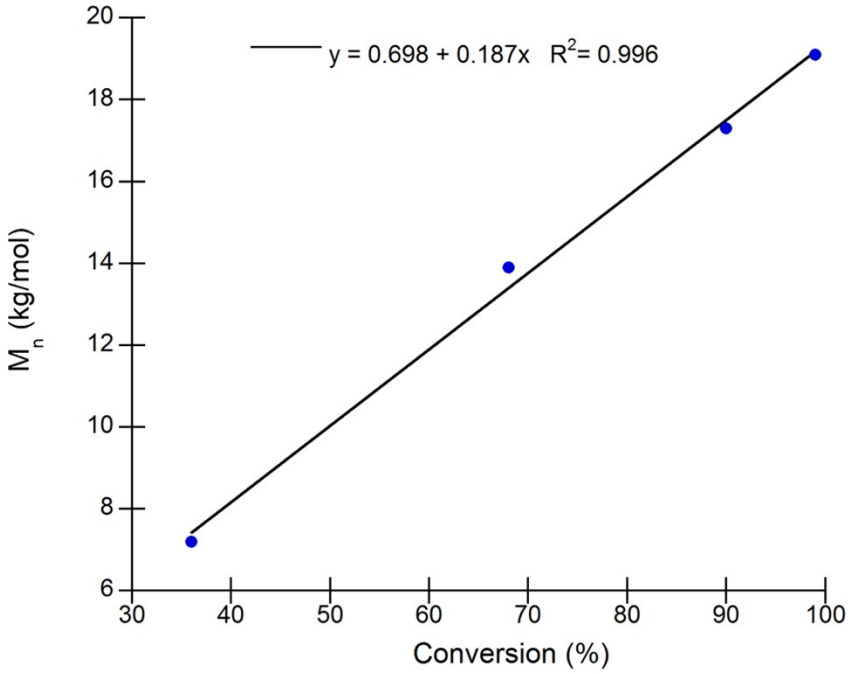

Figure S1. Molecular weight (M_n) vs. conversion for (*rac*)-lactide polymerization catalysed by **3b**.

Table S3. Attempted copolymerization of lactide (L) and ε-caprolactone (CL) in one pot.[a]

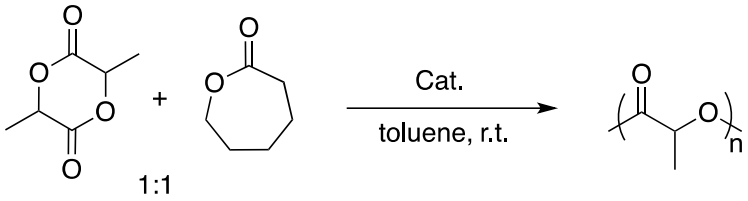

Entry	Cat.	Time (h)	Temp. (°C)	Conv. L (%)	Conv. CL (%)	M_n (kg/mol)	M_w/M_n
1	3b	9	24	95	0	85.0	1.40

[a]Reactions performed in toluene at 0.2 mol% catalyst loading. [Lactide] = [ε-caprolactone] = 0.34M.

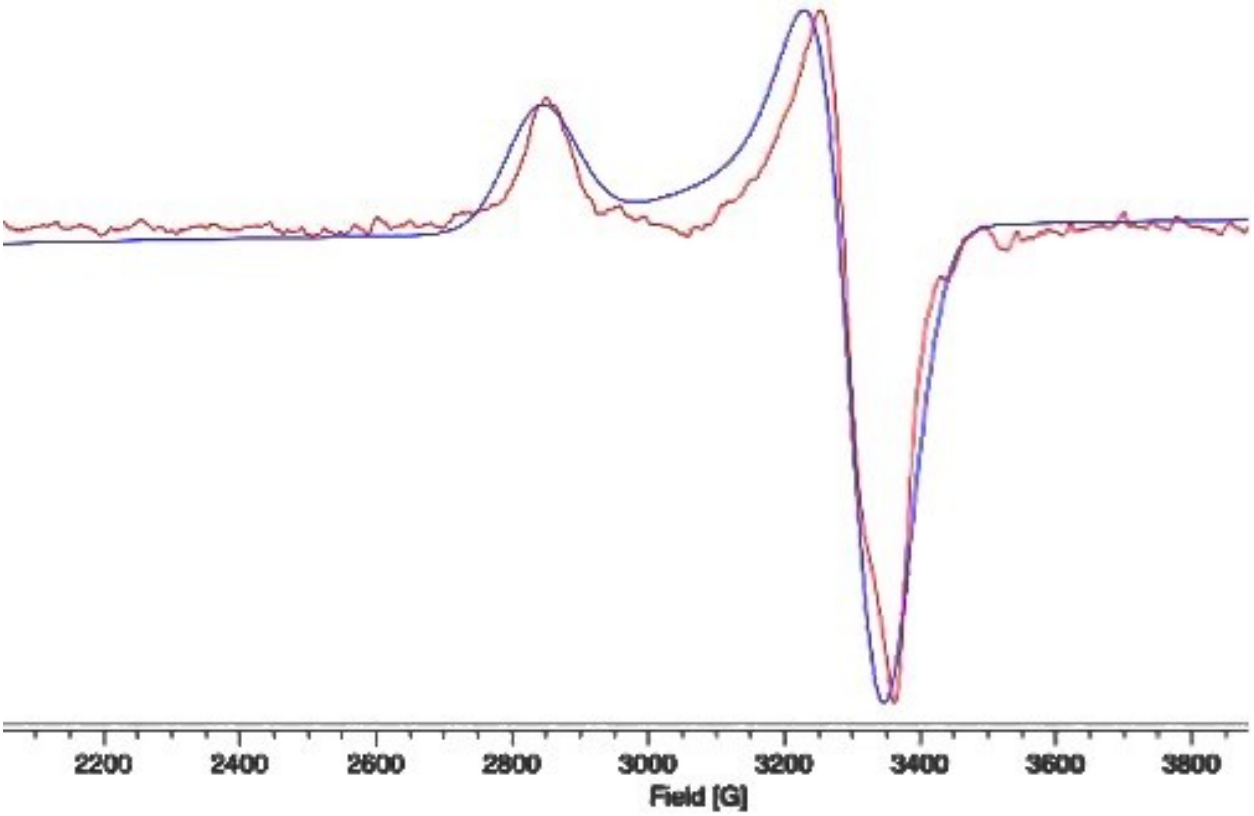

Figure S2. Frozen-toluene EPR spectrum of complex **3b** at 12K in red showing simulated spectrum in blue with the parameters given in the text.

An electron paramagnetic resonance spectrum of complex **3b** in a frozen toluene solution was collected and displayed an axial signal (g_{eff} = 2.04 and 2.37). This signal corresponds to an S = $^1/_2$ spin state (Figure S2). Notably, after comparison to a copper standard of >98% copper sulfate, it was determined that this $S = ^1/_2$ signal is coming from only 1% of the compound evaluated. Based on SQUID measurements we believe the compound has a spin state S = 3/2 spin states.

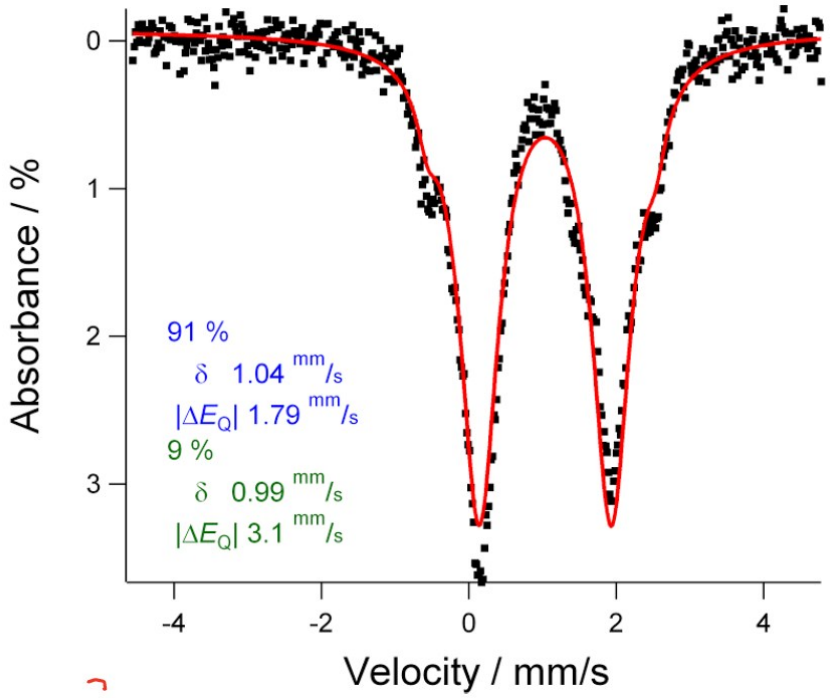

Figure S3. Zero field ^{57}Fe Mössbauer of **3a** at 90K.

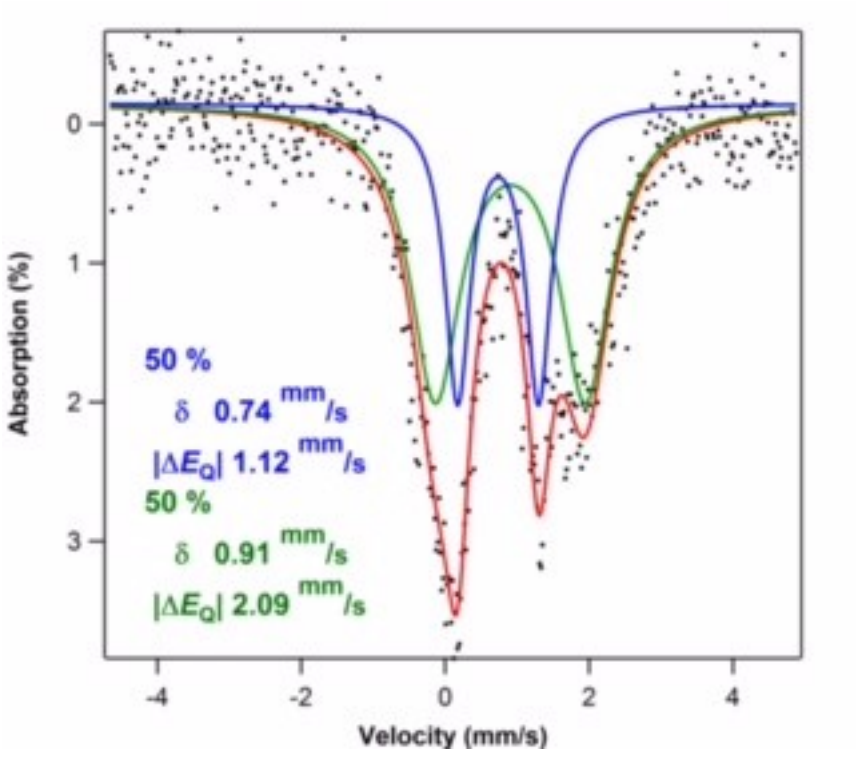

Figure S4. Zero field ^{57}Fe Mössbauer of **3a** at 90K when no precautions to prevent exposure to ether were taken.

Computational Details

Electronic structure. All calculations were performed at the density functional theory (DFT)[7] level with Gaussian 09.[8] Geometry optimizations were carried using the M06-L local density functional.[9,10] Numerical integrations were performed with an ultrafine grid. An automatic density-fitting set generated by the Gaussian program was employed to reduce the computational cost. Def2-TZVP basis sets were used for all atoms.[11] Selected species were re-optimized at TPSSh-D3BJ[12-14] level. Single point calculations on M06-L geometries were computed using a variety of density functionals (DFs): τ-HCTH,[15] B3LYP-D3BJ,[13,14,16] MN15,[17] B97D3,[13,14,18] OPBE-D3BJ,[13,14,19,20] and TPSSh-D3BJ.[12-14] Some of these DFs have been recommended for complexes bearing redox non-innocent ligands[21] and iron spin-state splitting energies.[22]

All quartet and doublet energies were corrected from spin contamination through sextet single point calculations following the Yamaguchi broken-spin-symmetry procedure,[23]

$$LSE = \frac{BSE\left(HS\langle S^2\rangle - LS\langle S^2\rangle\right) - HSE(BS\langle S^2\rangle - LS\langle S^2\rangle)}{HS\langle S^2\rangle - BS\langle S^2\rangle}$$

where $^{HS}\langle S^2\rangle$ and $^{BS}\langle S^2\rangle$ refer to the computed expectation values of the total spin operator for sextet (HS) and quartet or doublet (BS), and $^{LS}\langle S^2\rangle$ corresponds to the ideal expectation value of the total spin operator for quartet (3.75) or doublet (0.75).

Mulliken spin density surfaces are displayed with an isovalue of 0.006. Figure S4 shows the spin densities for quartet and doublet **3a** and **3b** at M06-L level.

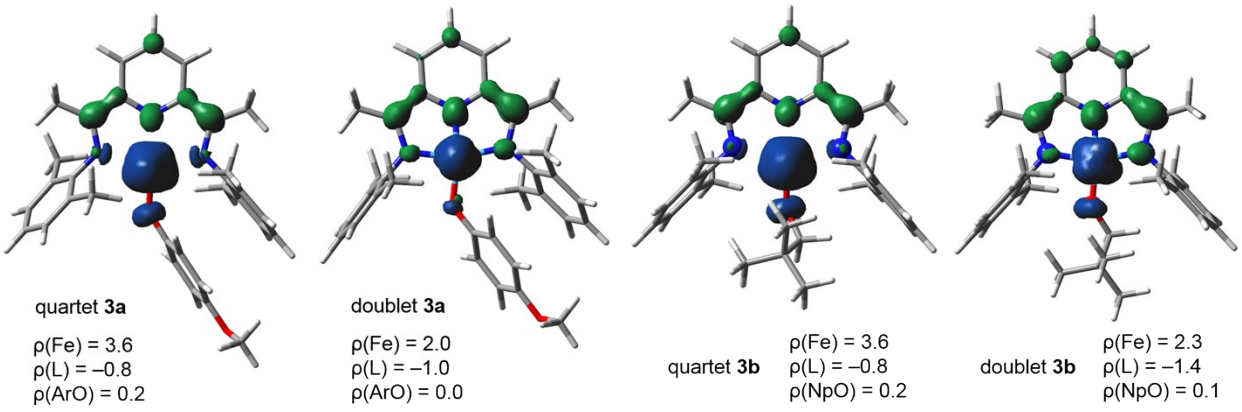

Figure S5. M06-L Mulliken spin densities for **3a** and **3b**.

Sensitivity of spin-state energetics. Table S4 collects the energies in kcal mol^{-1} for sextet, quartet, and doublet spin states of M06-L-optimized **3a** at different levels of theory. A graphical summary on the spin-state splitting energies between doublet and quartet states is shown in Figure S5.

Table S4. Spin-state energies (kcal mol^{-1}) of M06-L-optimized **3a**.

Density Functional	E_{sextet}	$E_{quartet}$	$E_{doublet}$
M06-L	7.6	0.0	5.6
τ-HCTH	9.0	0.0	3.6
B3LYP-D3BJ	4.2	0.0	3.2
MN15	5.3	0.0	−1.4
B97D3	9.0	0.0	−1.7
OPBE-D3BJ	10.5	0.0	−5.1
TPSSh-D3BJ	6.0	0.0	−6.4

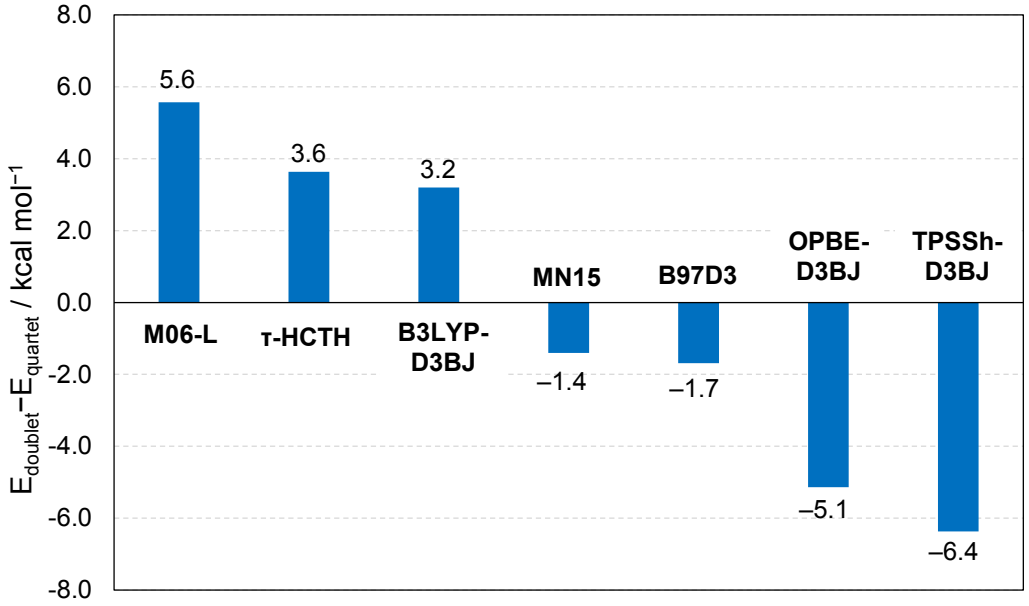

Figure S6. Spin-state splitting energies according to different density functionals.

Sensitivity of geometries. All species were optimized at M06-L level, which predicts a quartet ground state. To address the influence of the density functional on the geometry, we re-optimized species **3a** using TPSSh-D3BJ, a density functional that favors a doublet ground state

(Table S4). Selected bond distances and angles are collected in Table S5. Despite the somehow smaller O–Fe–N2 angle shown by TPSSh-D3BJ, the computed bond distances are quite similar and follow the same trend; shorter values are predicted for the doublet state.

Table S5. Selected bond distances and angles for M06-L- and TPSSh-D3BJ-optimized **3a**.

	M06-L		**TPSSh-D3BJ**	
Metric	quartet **3a**	doublet **3a**	quartet **3a**	doublet **3a**
d(Fe–N2) / Å	2.024	1.854	1.965	1.856
d(Fe–N1) / Å	2.122	1.970	2.055	1.927
d(Fe–N3) / Å	2.113	1.969	2.055	1.965
d(Fe–O) / Å	1.858	1.858	1.873	1.825
a(O–Fe–N2) / °	164.6	170.4	144.1	172.9
a(N1–Fe–N3) / °	149.0	160.4	142.7	160.8

^{57}Fe Mössbauer calculations. ^{57}Fe Mössbauer parameters (isomer shift δ and quadrupole splitting ΔE_Q) were computed following the procedure reported by Neese et al.[24,25] For the prediction of isomer shifts we first need to correlate theoretical electron densities ρ_0 with experimental isomer shifts δ_{exp}. Figure S6 collects the species used for this calibration. We employed most of the species of the calibration set reported by Neese et al.[25] plus two additional iron complexes **S** and **T**. **S** (δ = 1.13 mm/s)[26] was considered as an example of bis(imino)pyridine complex, whereas **T** (δ = −0.32 mm/s)[27] was included to expand the under-represented section of negative isomer shift values within the calibration set.

All calculations were carried out at the density functional theory using the M06-L local density functional as implemented in ORCA.[28] Geometry optimizations were performed with Def2-TZVP basis sets for all atoms; subsequent single point calculations were performed with Def2-TZVPP for Fe and Def2-TZVPPD for the rest of atoms.[11,29] Def2-TZVP/J auxiliary basis sets were employed. We used an integration accuracy of 11 for Fe and 7 for the rest of atoms. All calculations regarding the calibration set were carried out in an aqueous environment[25] using the COSMO model.[30] Complexes **3a** and **3b** were reoptimized in SMD=water[31] as implemented in Gaussian 09 and the resulting geometries were used to compute ρ_0 and ΔE_Q using the above-mentioned procedure in ORCA.

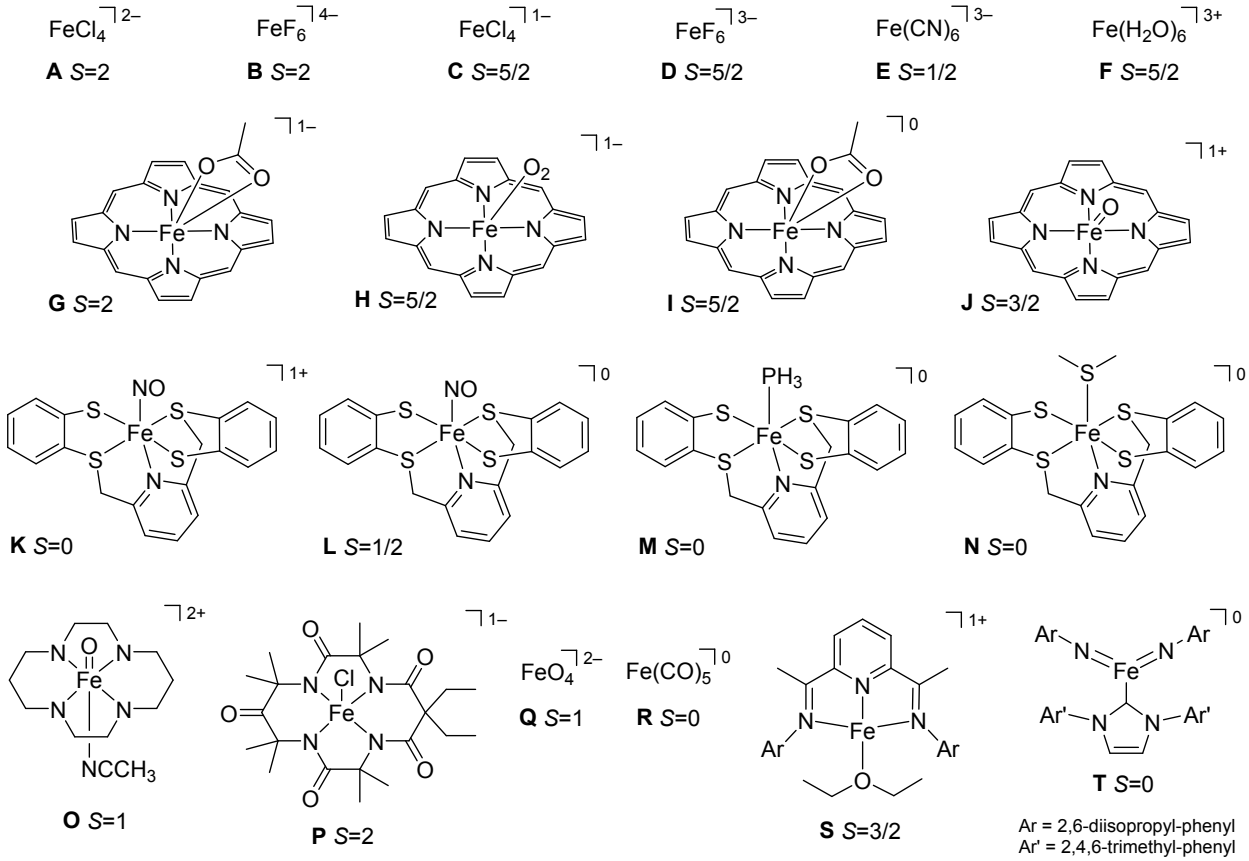

Figure S7. Species used for the calibration of ^{57}Fe Mössbauer isomer shifts.

Table S6. Calculated electron densities ρ_0 and experimental isomer shifts δ_{exp}.

Species	ρ_0 / a.u.$^{-3}$	δ_{exp} / mm/s	Species	ρ_0 / a.u.$^{-3}$	δ_{exp} / mm/s
A	11583.130	0.90	**K**	11584.812	0.04
B	11581.592	1.34	**L**	11584.051	0.33
C	11585.063	0.19	**M**	11583.844	0.34
D	11583.942	0.48	**N**	11583.531	0.44
E	11586.138	−0.13	**O**	11584.261	0.17
F	11583.877	0.50	**P**	11584.975	−0.02
G	11583.027	1.05	**Q**	11588.968	−0.87
H	11583.338	0.67	**R**	11586.136	0.00
I	11583.829	0.40	**S**	11582.126	1.13
J	11584.892	0.08	**T**	11586.677	−0.32

Figure S8 plots the regression line between experimental isomer shifts and calculated electron densities at the iron nucleus. The calibration equation for the calculation of isomer shifts results as follows:

$$\delta = \alpha(\rho_0 - C) + \beta = -0.303 \cdot (\rho_0 - 11580) + 1.667$$

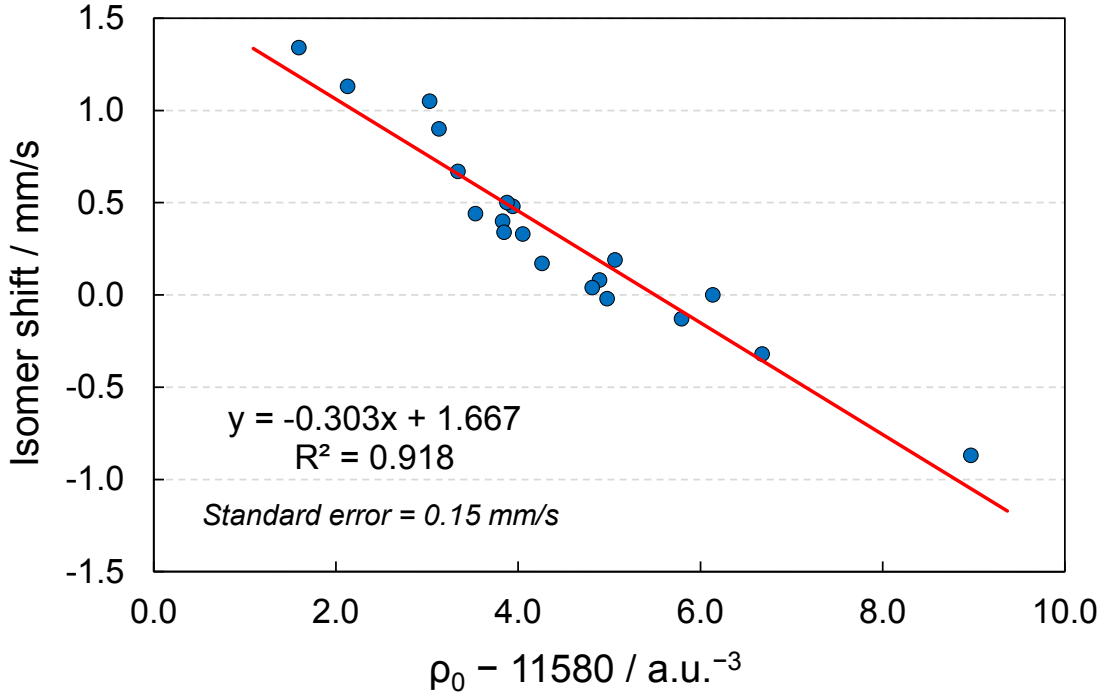

Figure S8. Correlation between experimental isomer shifts and calculated electron densities.

Table S7. Calculated ρ_0, δ, and ΔE_Q for **3a** and **3b**.

Species	**ρ_0 / a.u.$^{-3}$**	**δ / mm/s**	**ΔE_Q / mm/s**
3a *S*=3/2	11582.664	0.86	1.159
3a *S*=1/2	11583.429	0.63	2.224
3b *S*=3/2	11582.720	0.84	1.361
3b *S*=1/2	11583.576	0.58	2.304

Electronic energies and coordinates for all species.

For XYZ coordinates, see attached file *coordinates.xyz*

Table S8. Electronic energies (hartrees) for geometries at M06-L level.

Species	DF	Energy	Species	DF	Energy
3a *S*=1/2	M06-L	-2818.721437 -2818.696482[a]	**3a** *S*=3/2	M06-L	-2818.730379 -2818.718871[a]
	τ-HCTH	-2819.136419 -2819.105267[a]		τ-HCTH	-2819.142895 -2819.129558[a]
	B3LYP-D3BJ	-2819.171976 -2819.144491[a]		B3LYP-D3BJ	-2819.178645 -2819.171065[a]
	MN15	-2817.183299 -2817.149535[a]		MN15	-2817.183307 -2817.174700[a]
	B97D3	-2818.473976 -2818.437096[a]		B97D3	-2818.472517 -2818.458837[a]
	OPBE-D3BJ	-2818.962387 -2818.927855[a]		OPBE-D3BJ	-2818.954244 -2818.940120[a]
	TPSSh-D3BJ	-2819.215572 -2819.176784[a]		TPSSh-D3BJ	-2819.207913 -2819.198663[a]
3a *S*=5/2	M06-L	-2818.720511	**3b** *S*=1/2	M06-L	-2669.669765 -2669.639089[a]
	τ-HCTH	-2819.130932	**3b** *S*=3/2	M06-L	-2669.679406 -2669.665862[a]
	B3LYP-D3BJ	-2819.173492	**3b** *S*=5/2	M06-L	-2669.668177
	MN15	-2817.176761	**3a** *S*=1/2[b]	TPSSh-D3BJ	-2819.217858
	B97D3	-2818.460454	**3a** *S*=3/2[b]	TPSSh-D3BJ	-2819.213850
	OPBE-D3BJ	-2818.939934			
	TPSSh-D3BJ	-2819.200118			

[a] Sextet single point energy to correct for spin contamination. [b] Geometries at TPSSh-D3BJ level.

Table S9. Electronic energies (hartrees) of the isomer shift calibration set.

Species	Def2-TZVP	Def2-TZVPPD	Species	Def2-TZVP	Def2-TZVPPD
A	-3105.072858	-3105.076691	**K**	-3774.425141	-3774.443409
B	-1863.594411	-1863.634405	**L**	-3774.577884	-3774.595993
C	-3104.927700	-3104.931625	**M**	-3987.782381	-3987.799609
D	-1863.569602	-1863.593558	**N**	-4122.666700	-4122.686668
E	-1821.416162	-1821.418563[a]	**O**	-2243.422430	-2243.445741
F	-1722.032964	-1722.061948	**P**	-3178.558098	-3178.579435
G	-2481.104755	-2481.121389	**Q**	-1564.924316	-1564.933501
H	-2402.933524	-2402.951218	**R**	-1830.619538	-1830.623599
I	-2480.975898	-2480.994563	**S**	-2945.382652	-2945.415471
J	-2327.404181	-2327.420003	**T**	-3232.920639	-3232.956475

[a] Def2-TZVPP basis set.

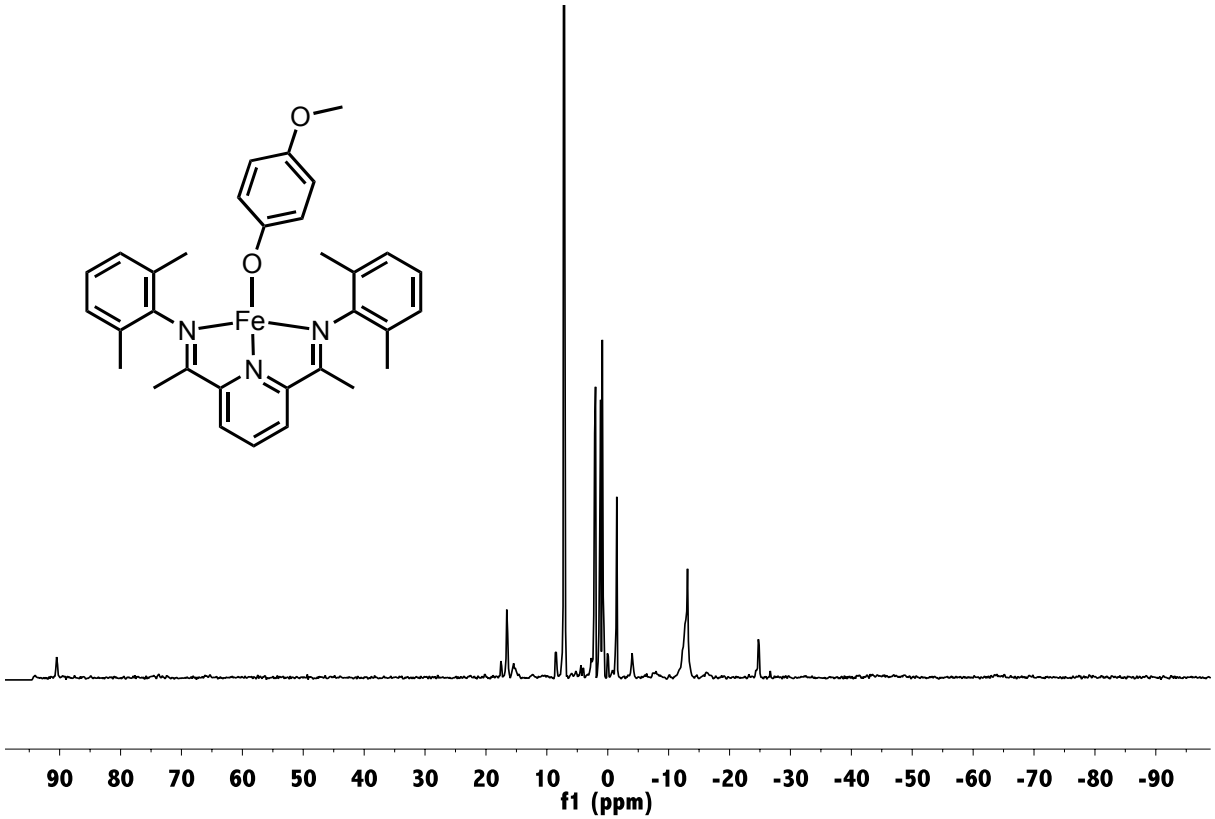

Figure S9. ^{1}H NMR spectrum of **3a** in C_6D_6 at 25 ºC.

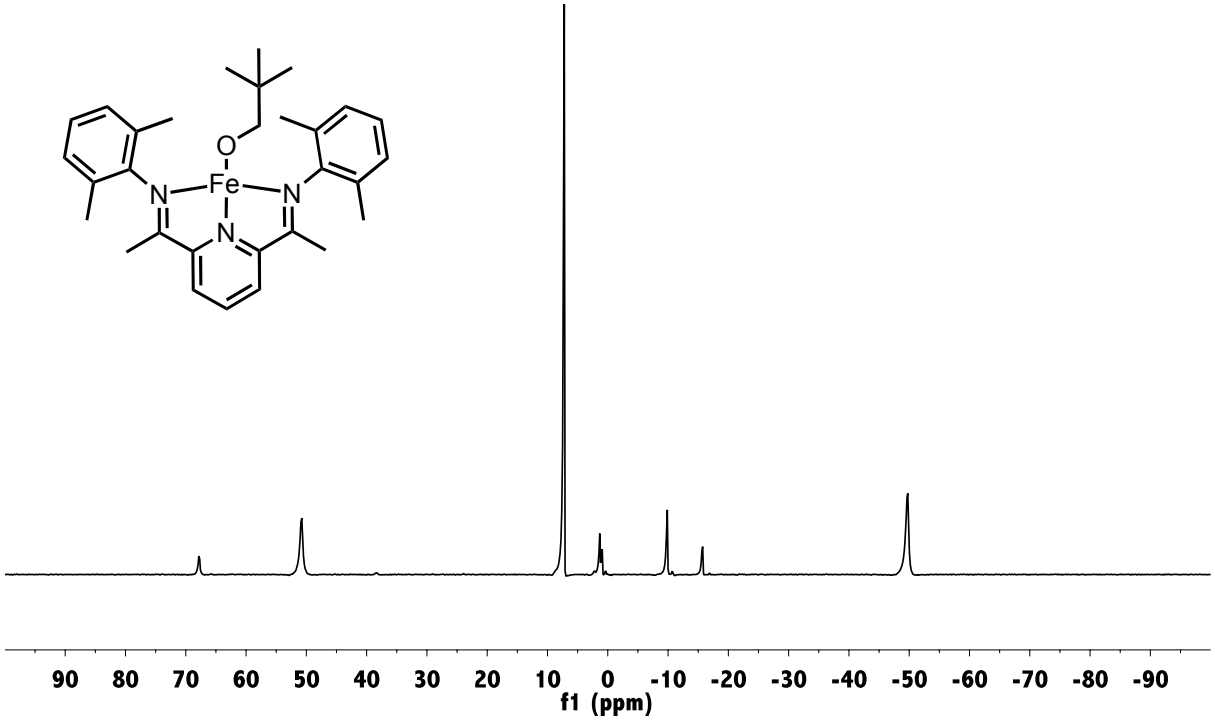

Figure S10. ^{1}H NMR spectrum of **3b** in C_6D_6 at 25 ºC.

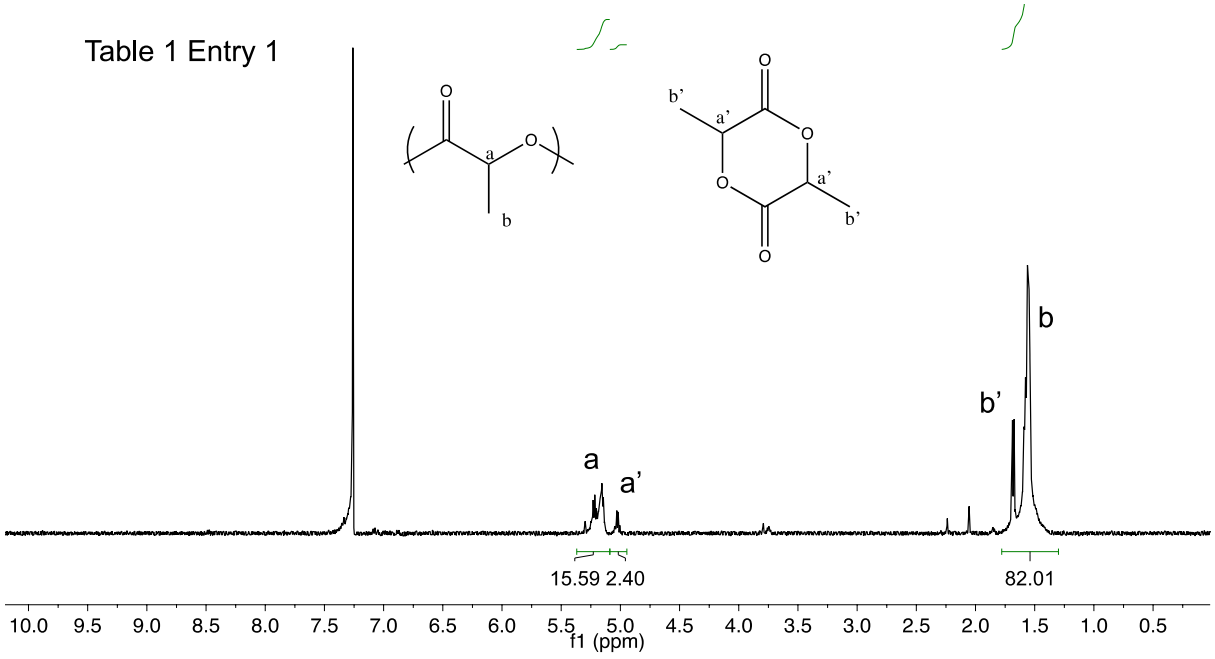

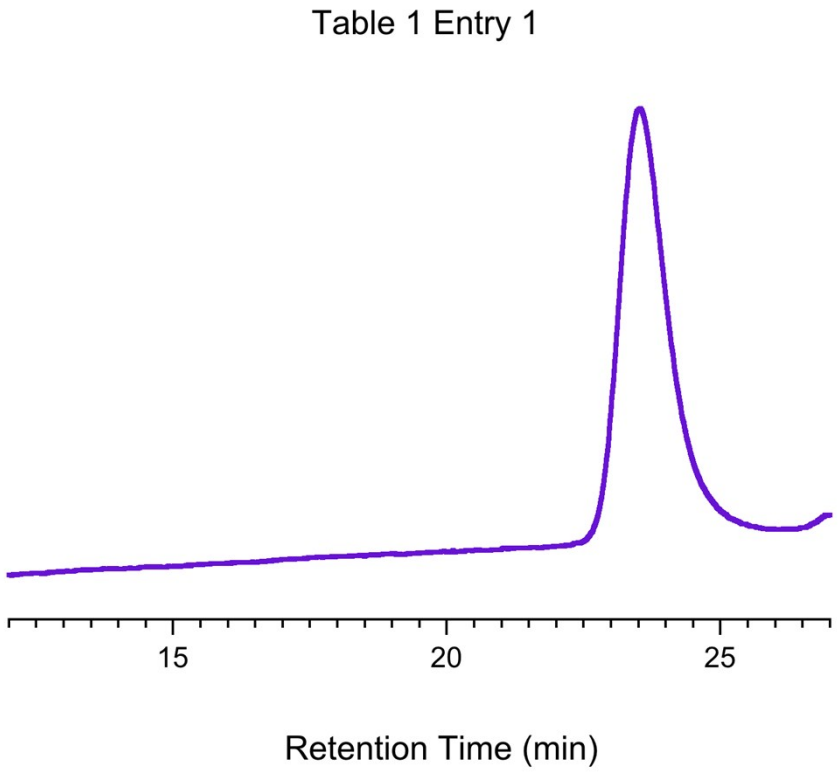

Figure S11. ^{1}H NMR and GPC trace of polymer from Table 1 Entry 1.

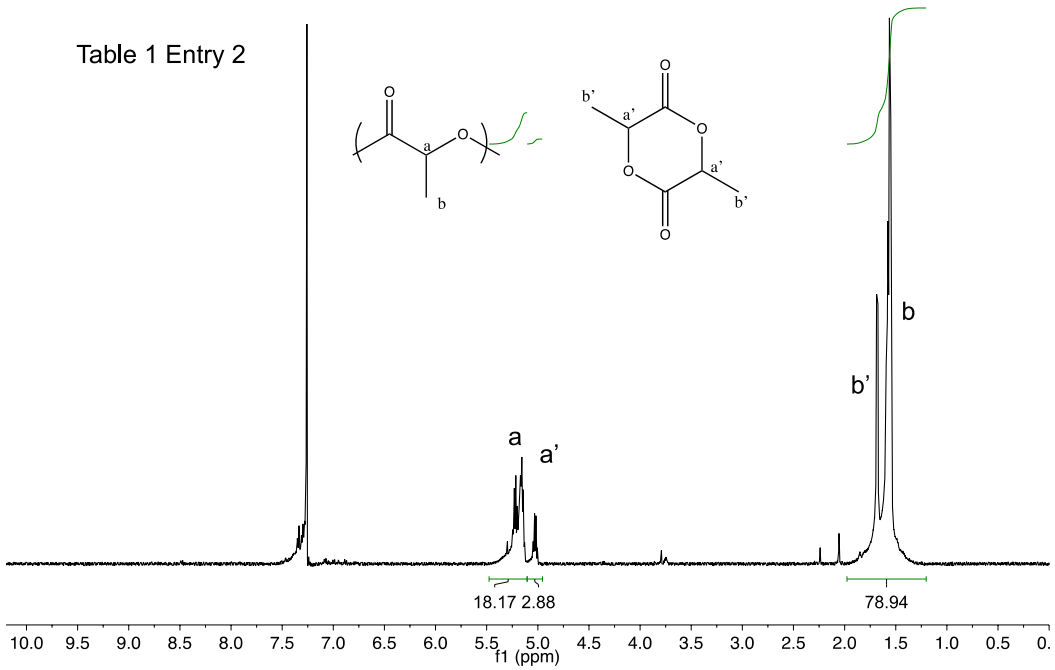

Table 1 Entry 2

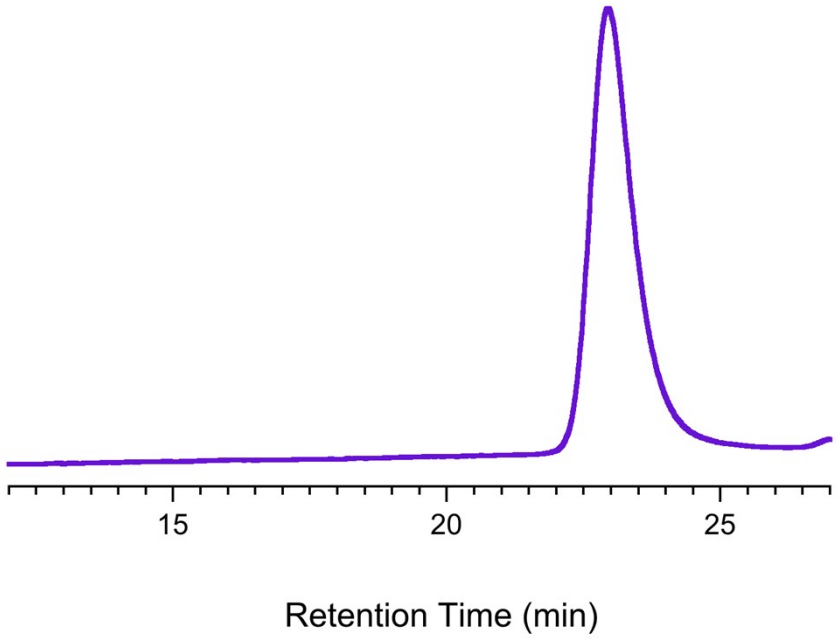

Figure S12. ^{1}H NMR and GPC trace of polymer from Table 1 Entry 2.

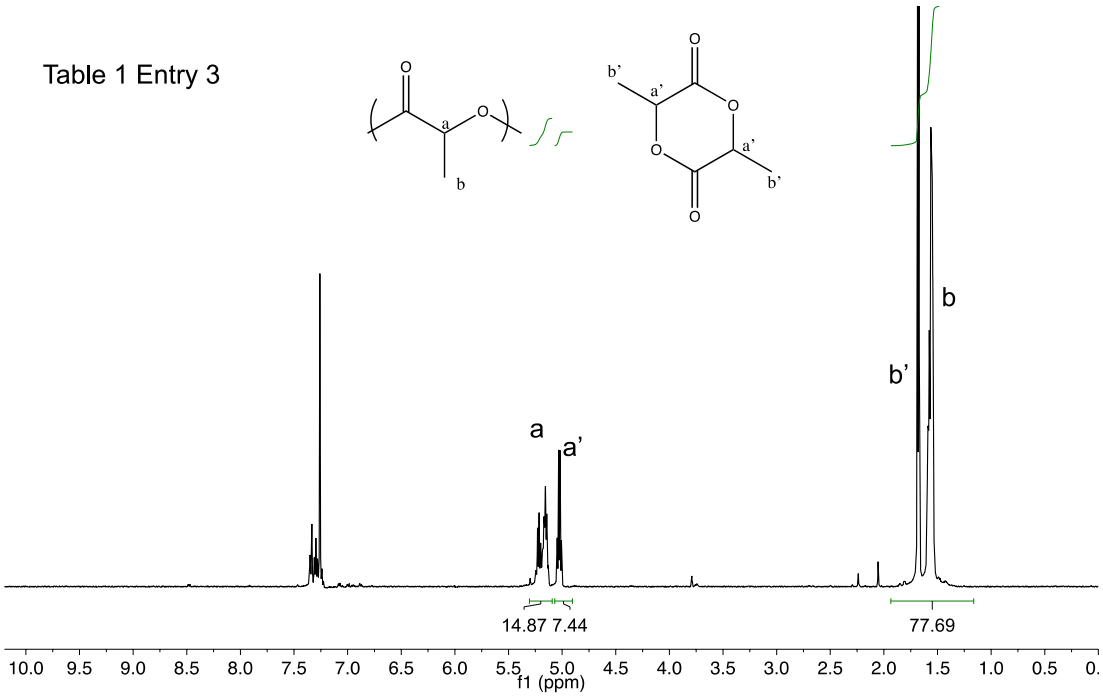

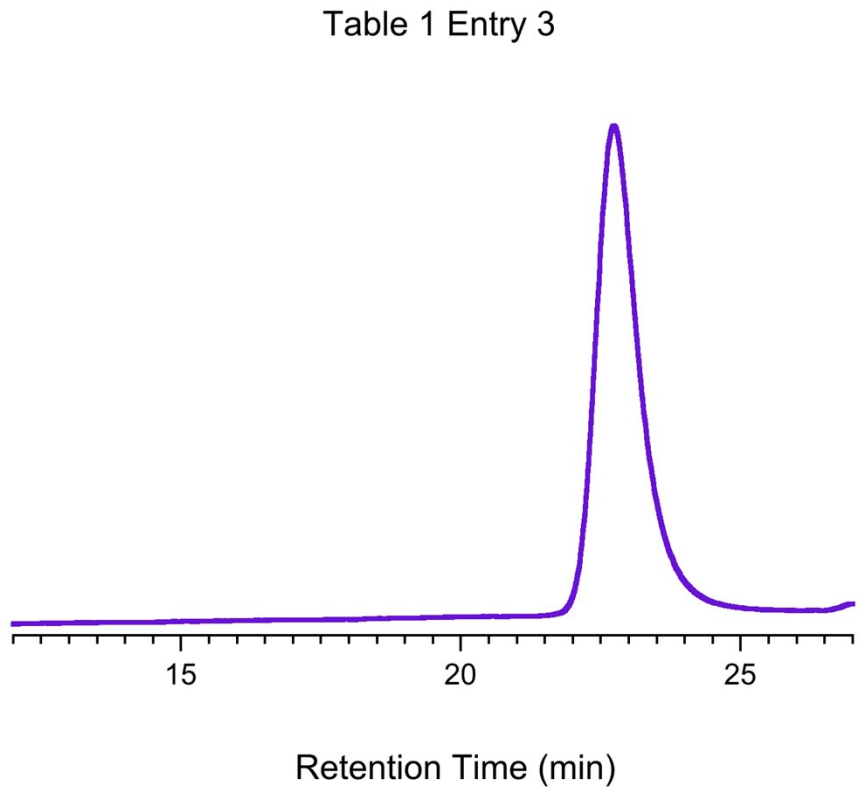

Figure S13. ^{1}H NMR and GPC trace of polymer from Table 1 Entry 3.

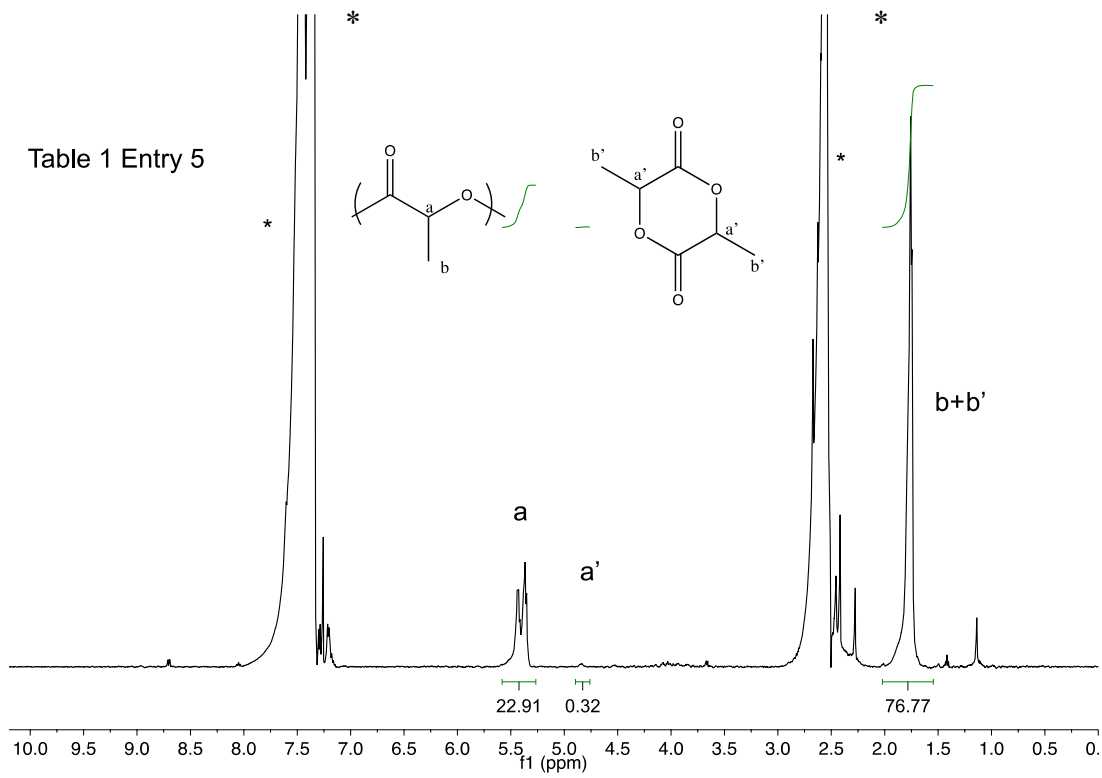

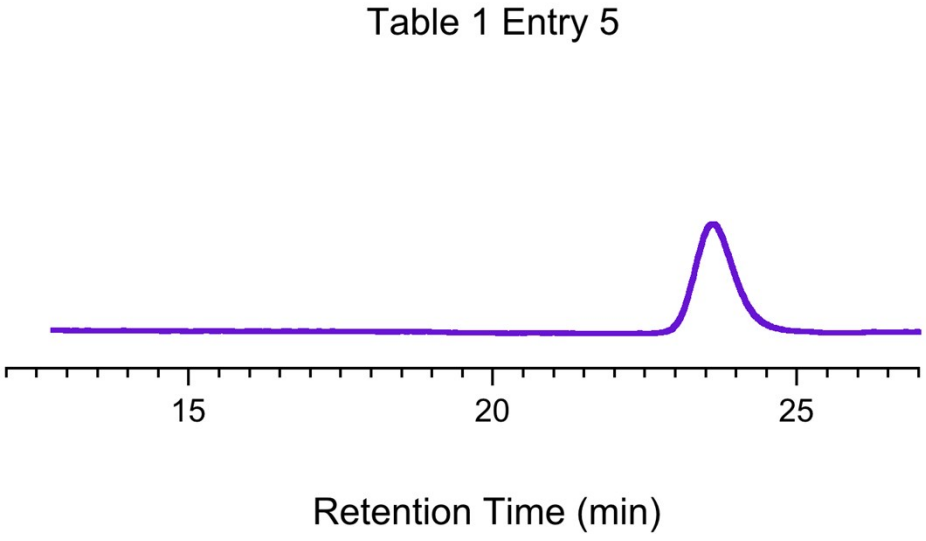

Figure S14. ^{1}H NMR and GPC trace of polymer from Table 1 Entry 5. *Toluene

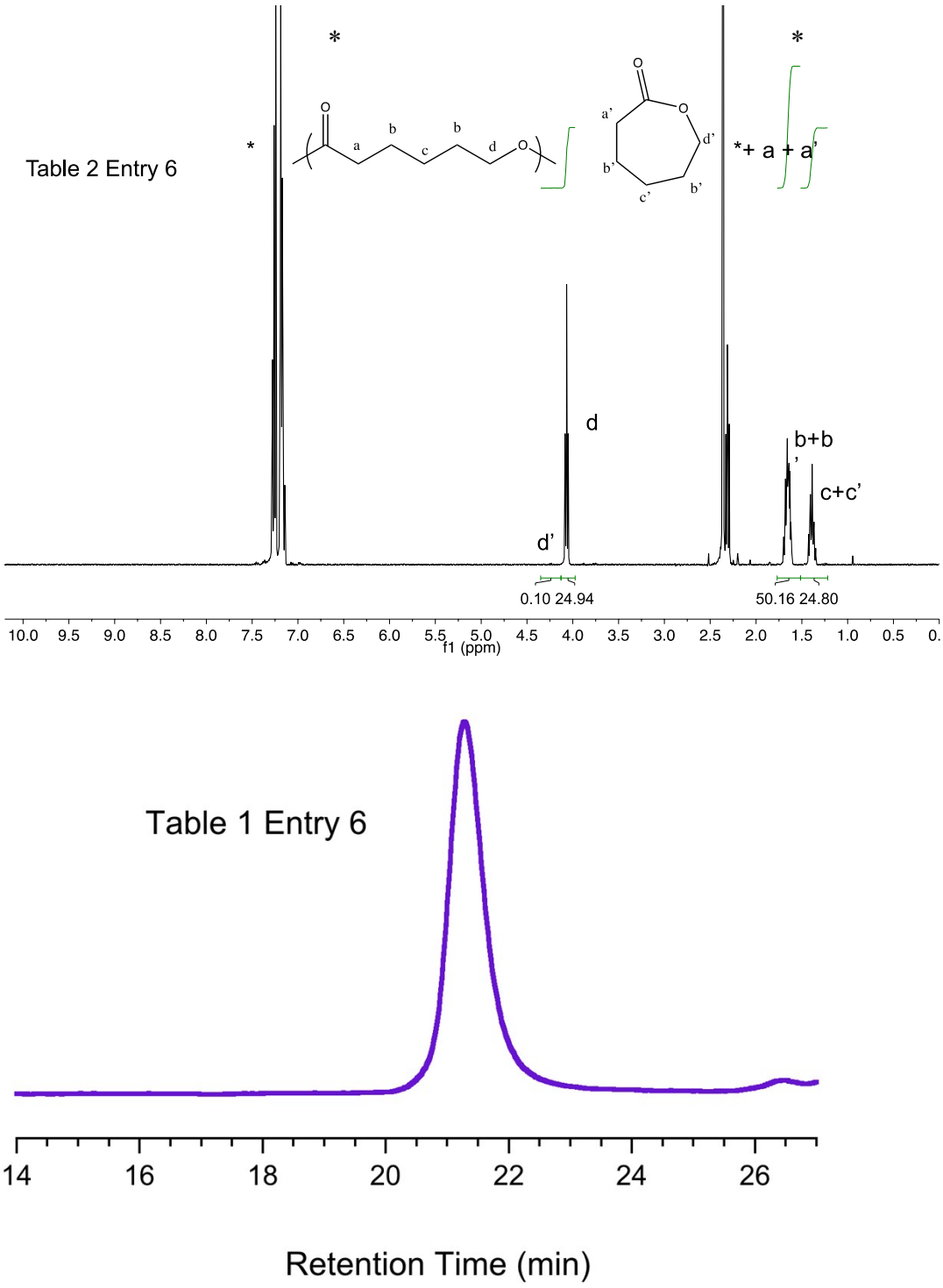

Figure S15. ^{1}H NMR and GPC trace of polymer from Table 1 Entry 6. *Toluene.

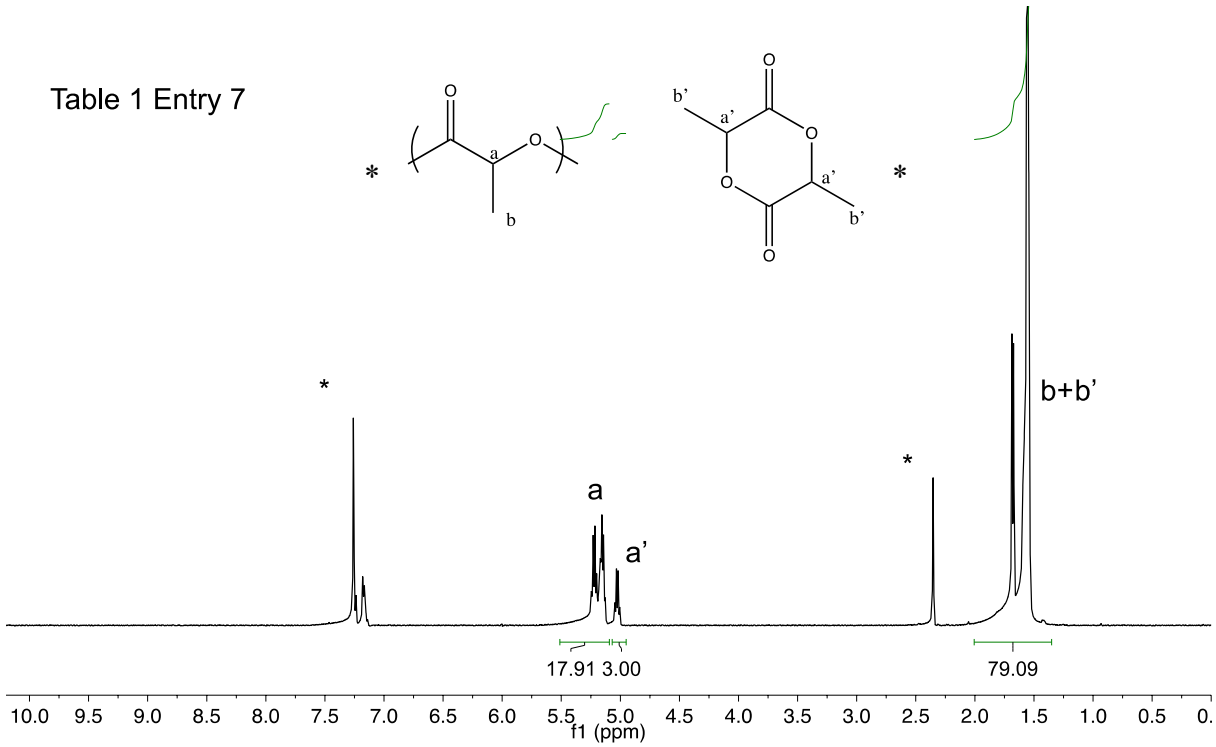

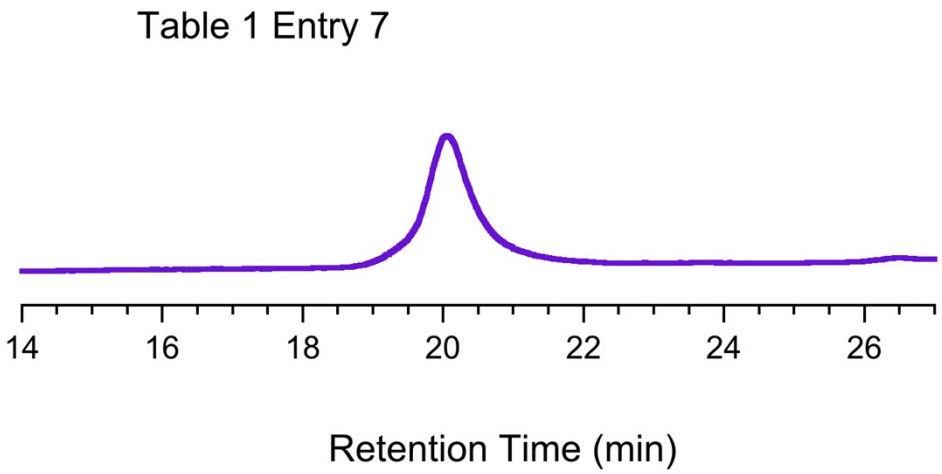

Figure S16. ^{1}H NMR and GPC trace of polymer from Table 1 Entry 7. *Toluene.

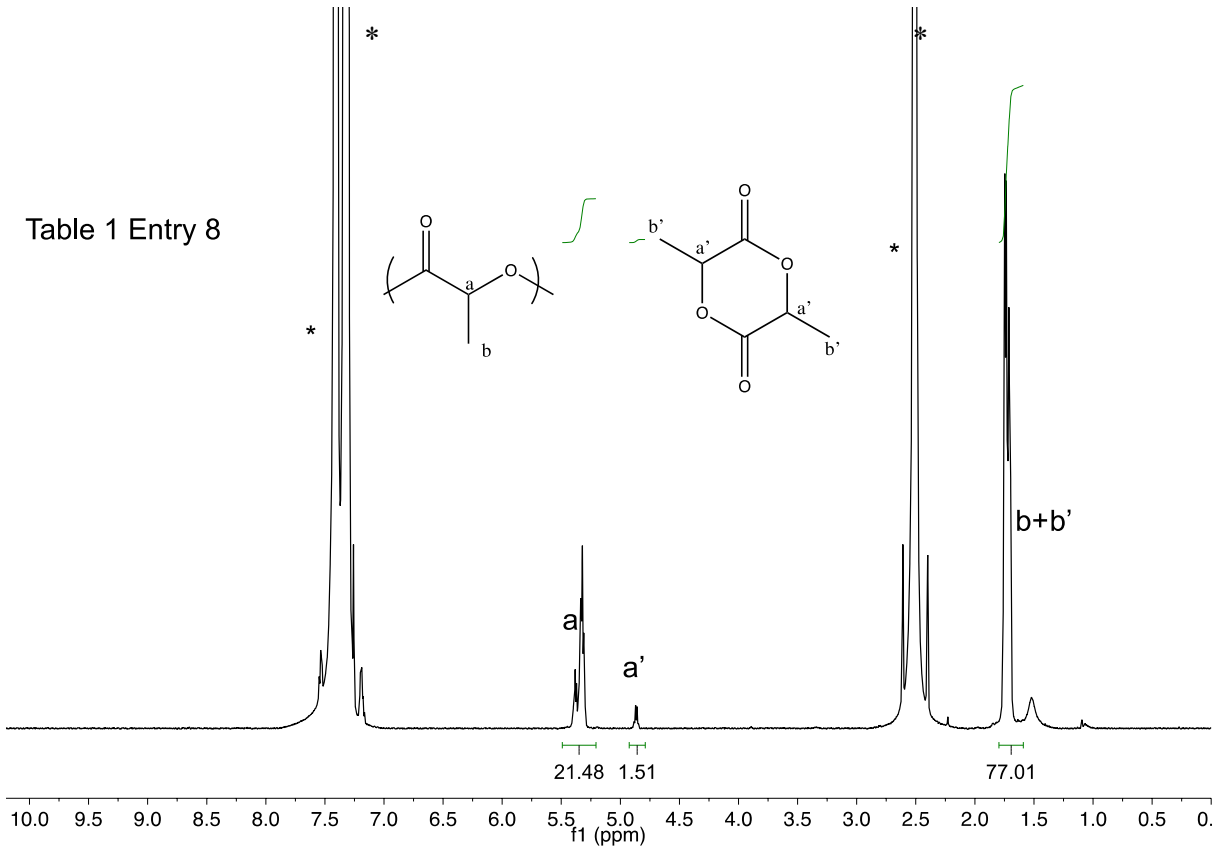

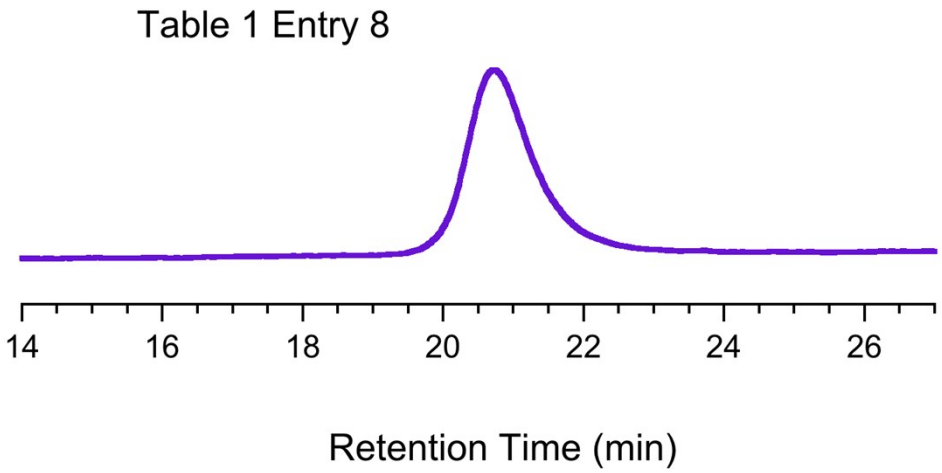

Figure S17. ^{1}H NMR and GPC trace of polymer from Table 1 Entry 8. *Toluene.

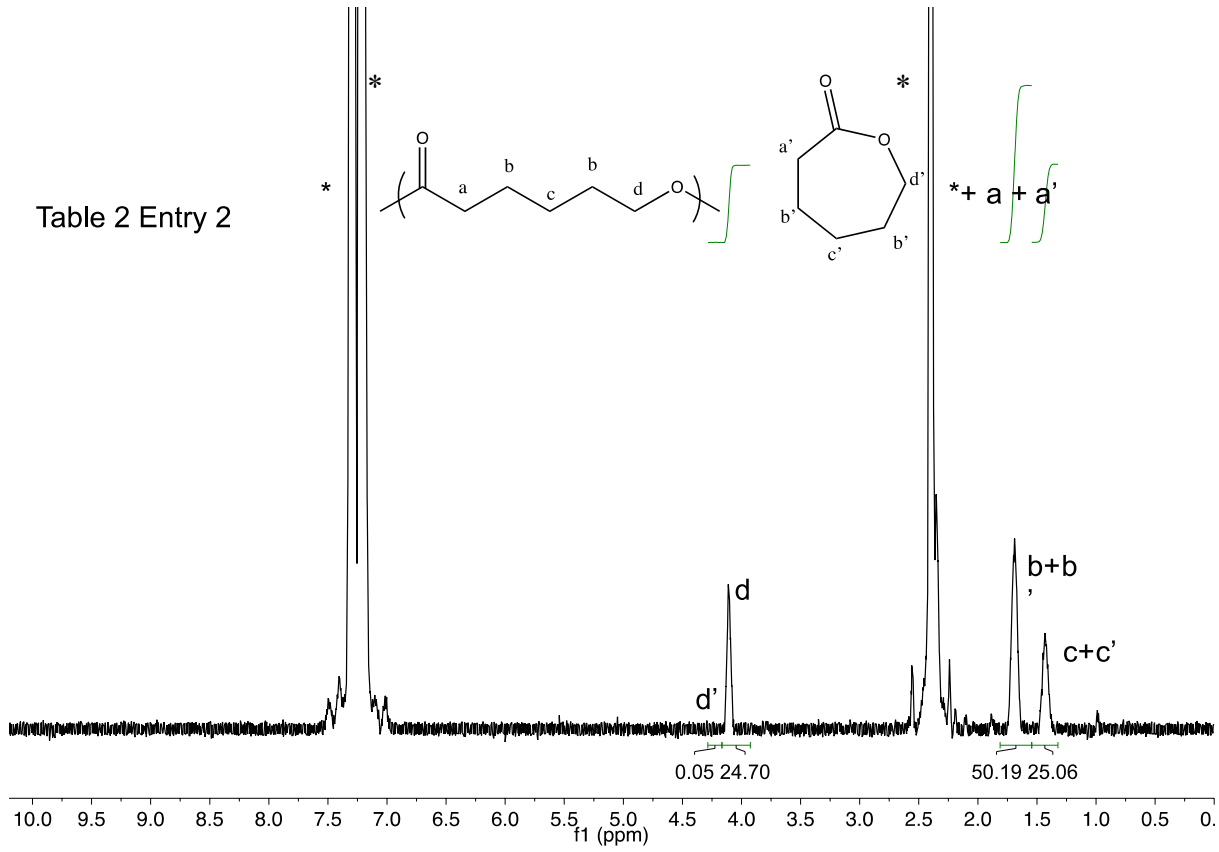

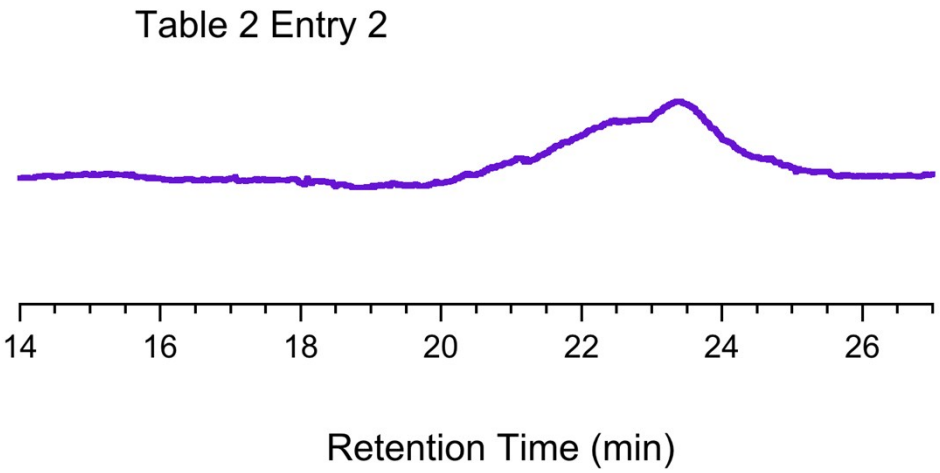

Figure S18. [1]H NMR and GPC trace of polymer from Table 2 Entry 2. *Toluene.

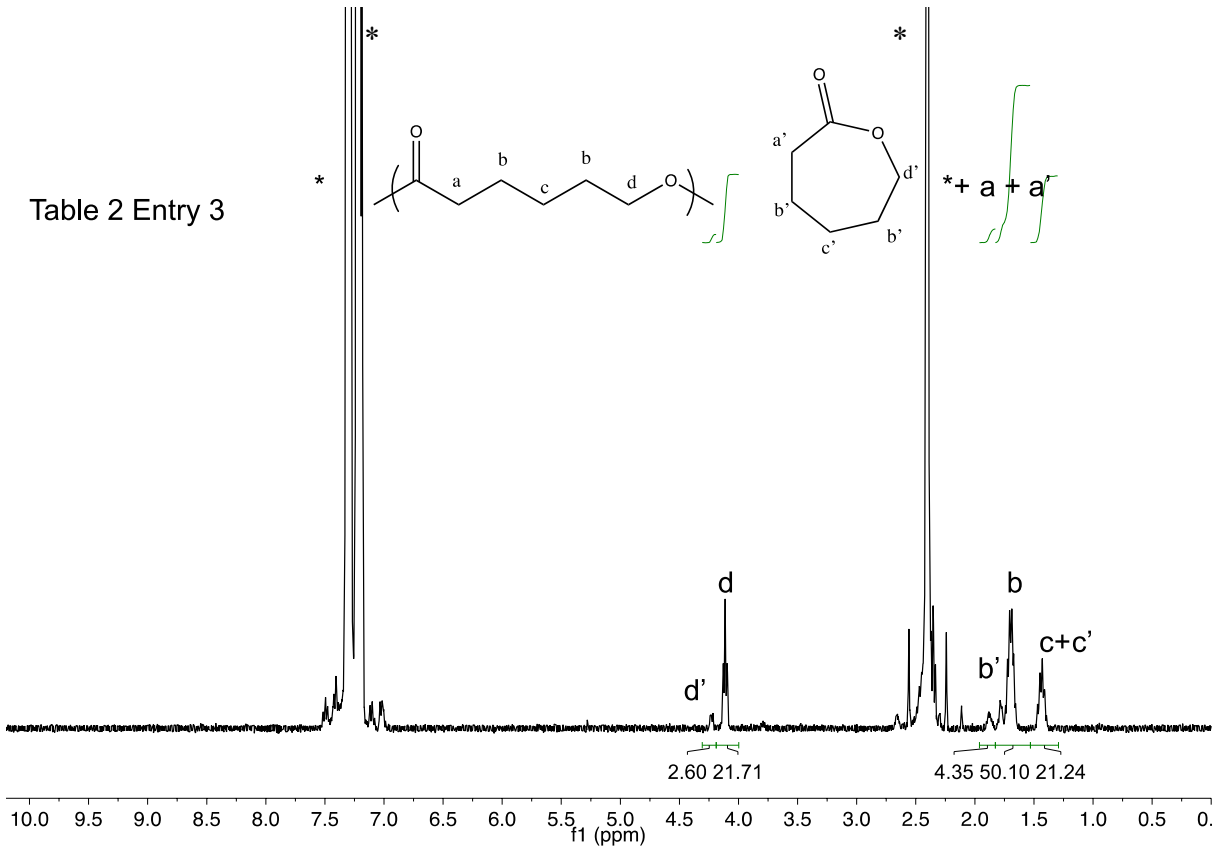

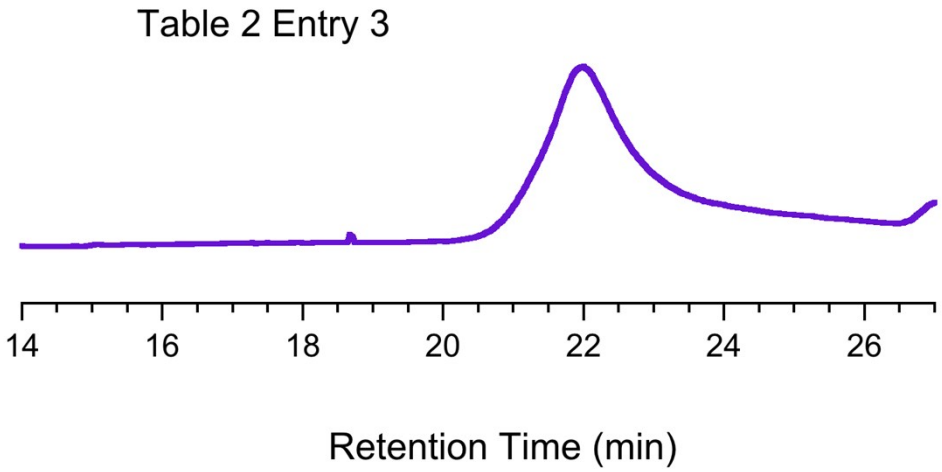

Figure S19. [1]H NMR and GPC trace of polymer from Table 2 Entry 3. *Toluene.

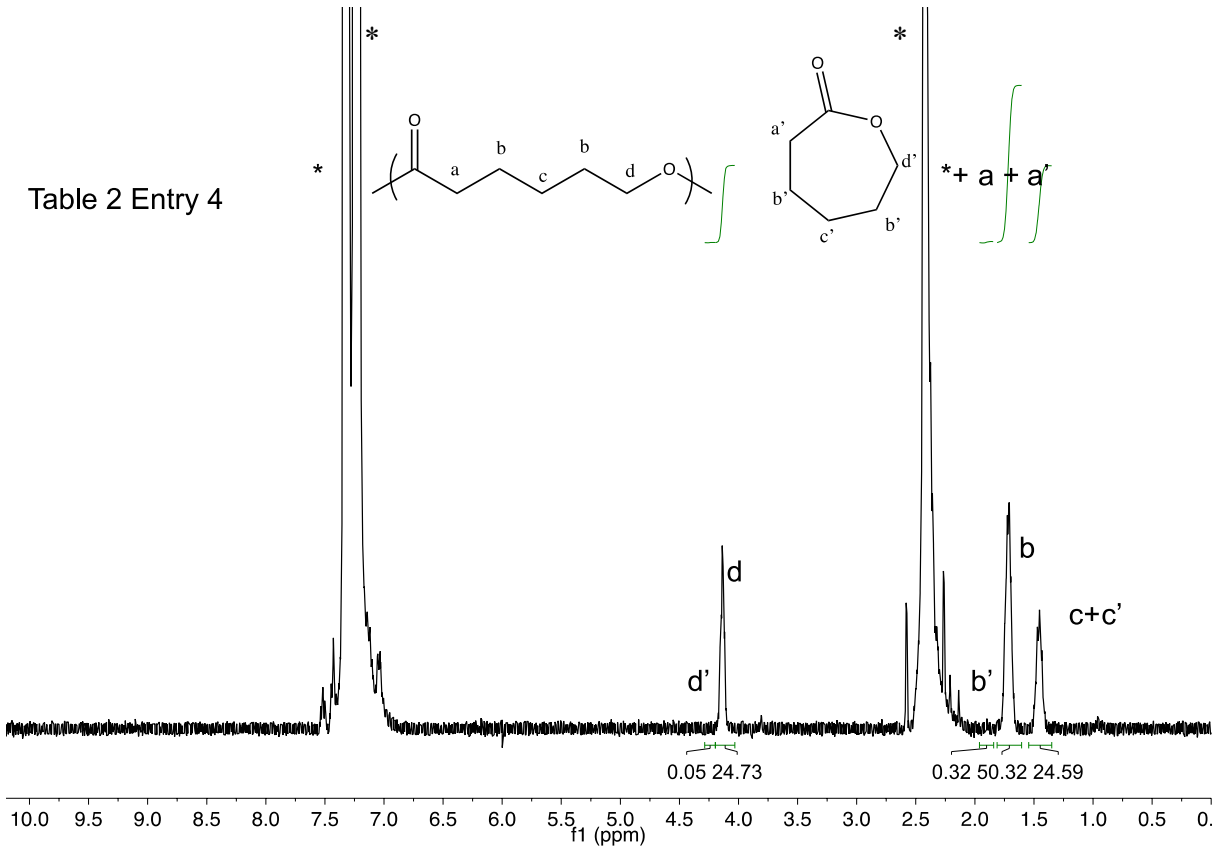

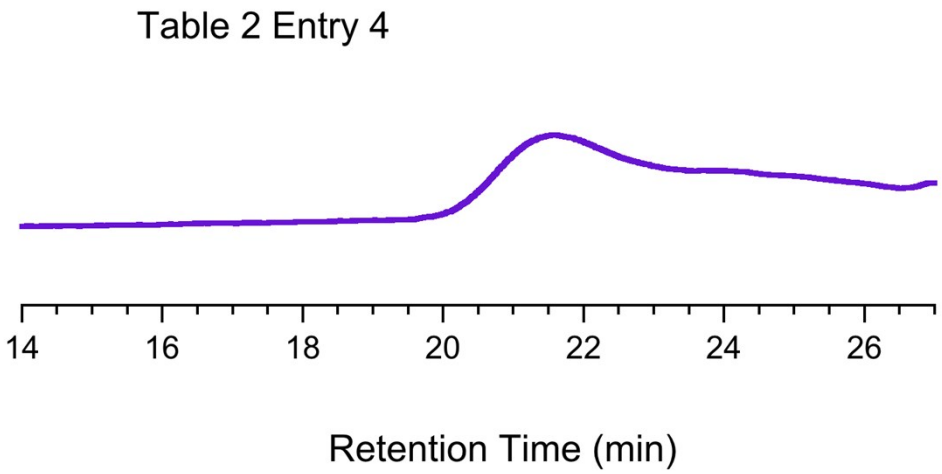

Figure S20. ^{1}H NMR and GPC trace of polymer from Table 2 Entry 4. *Toluene.

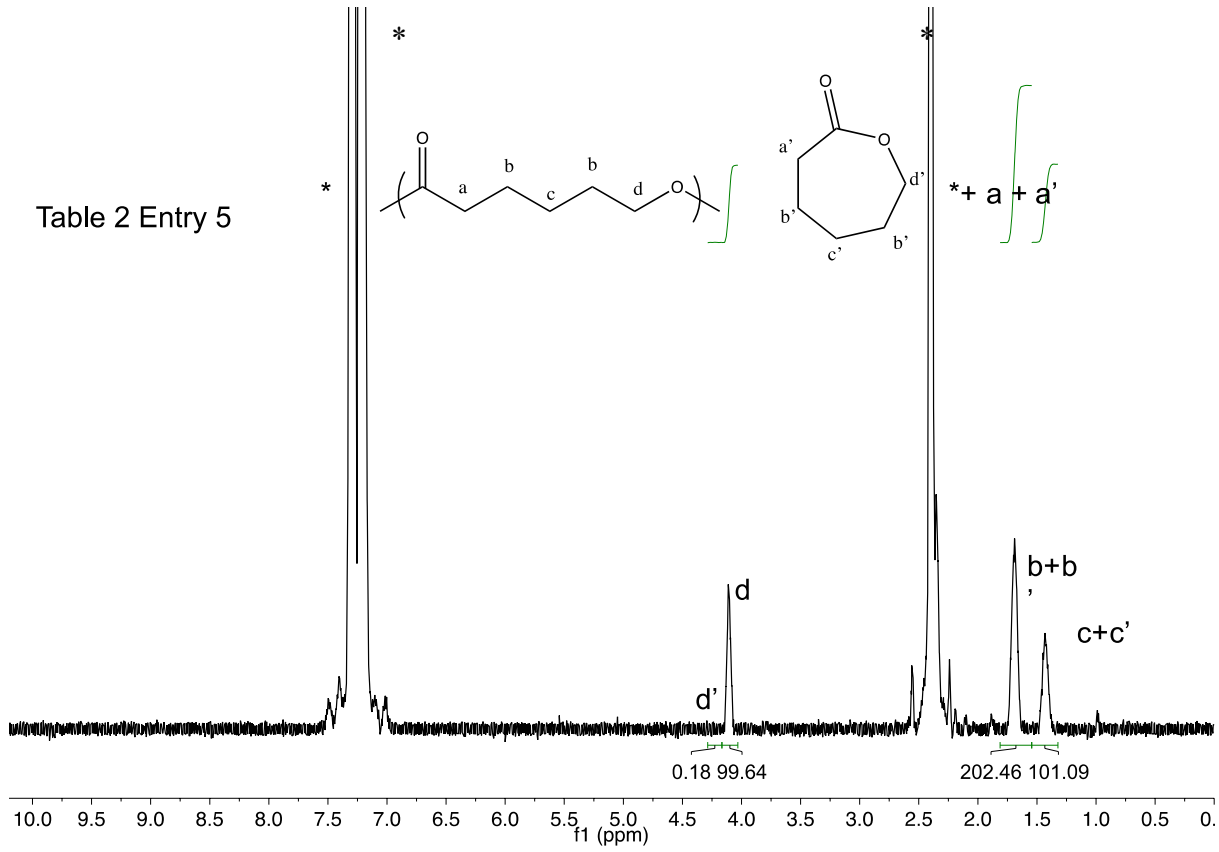

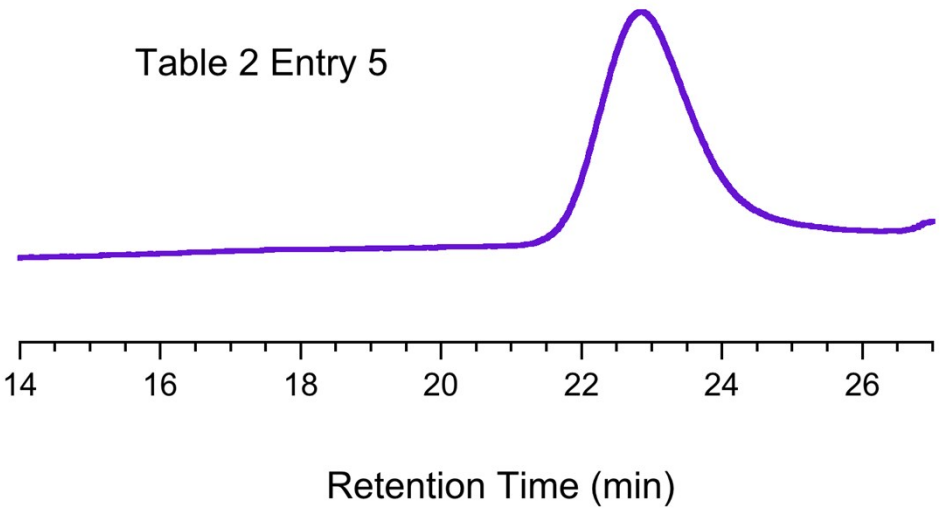

Figure S21. [1]H NMR and GPC trace of polymer from Table 2 Entry 5. *Toluene.

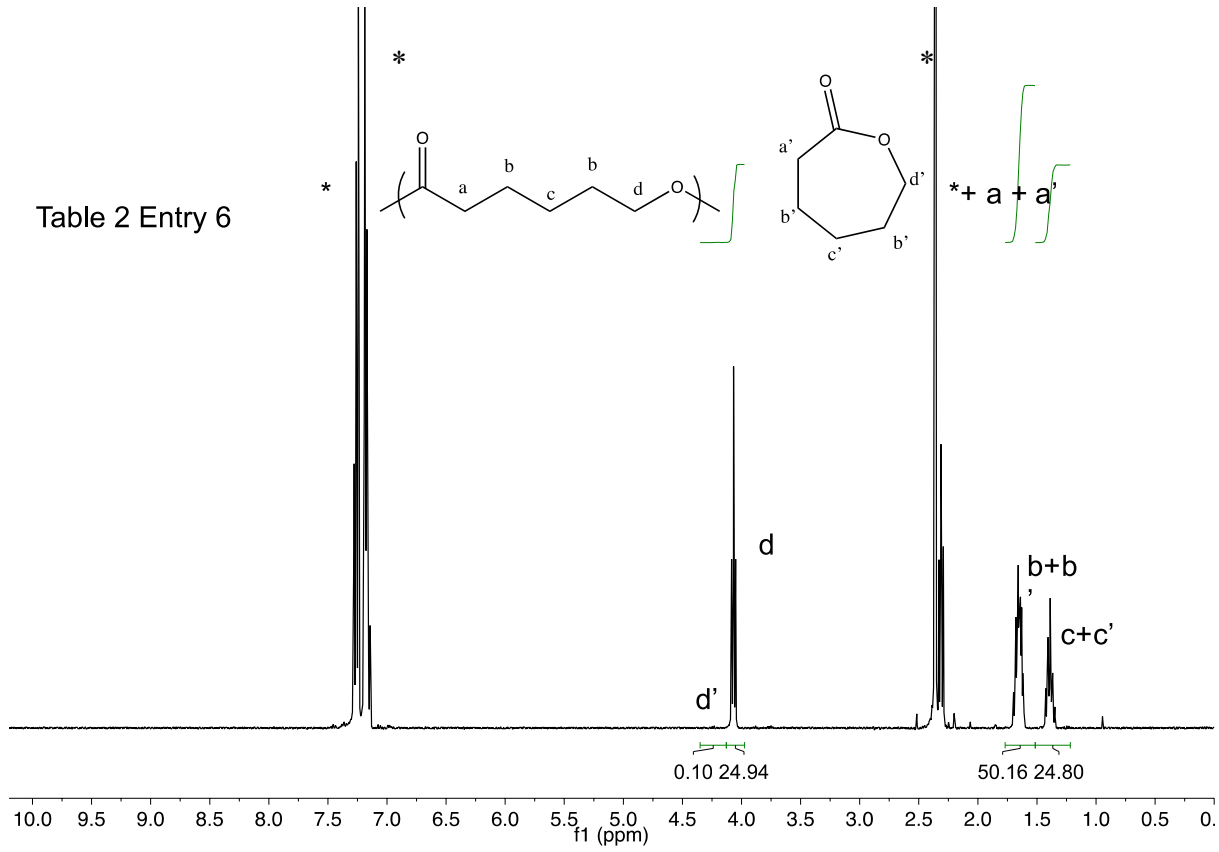

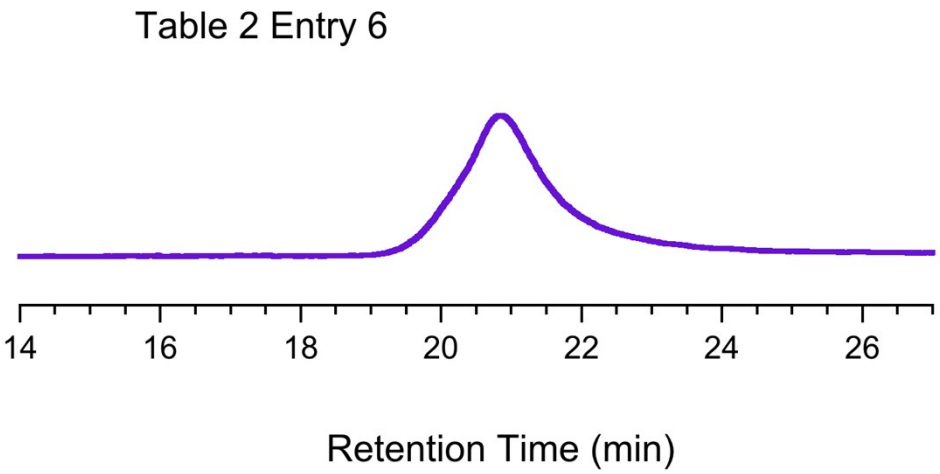

Figure S22. [1]H NMR and GPC trace of polymer from Table 2 Entry 6. *Toluene

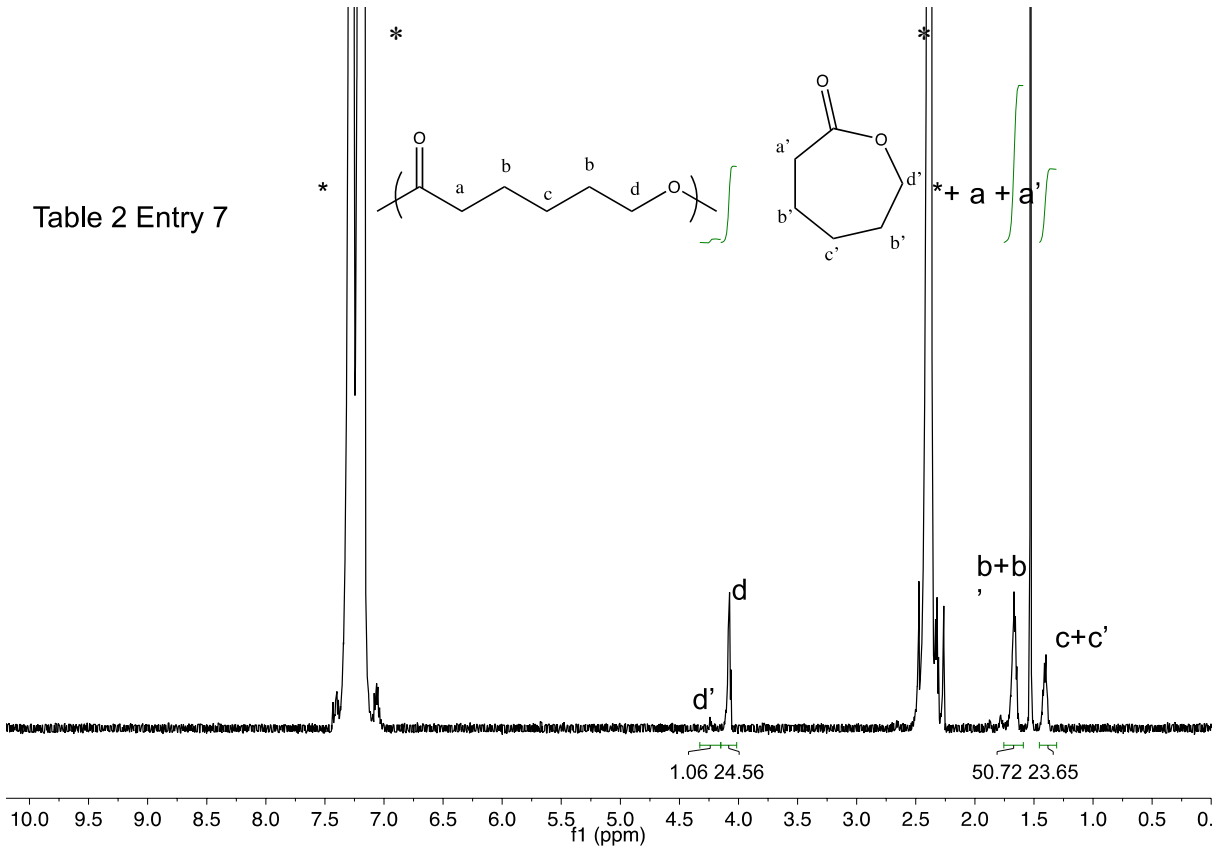

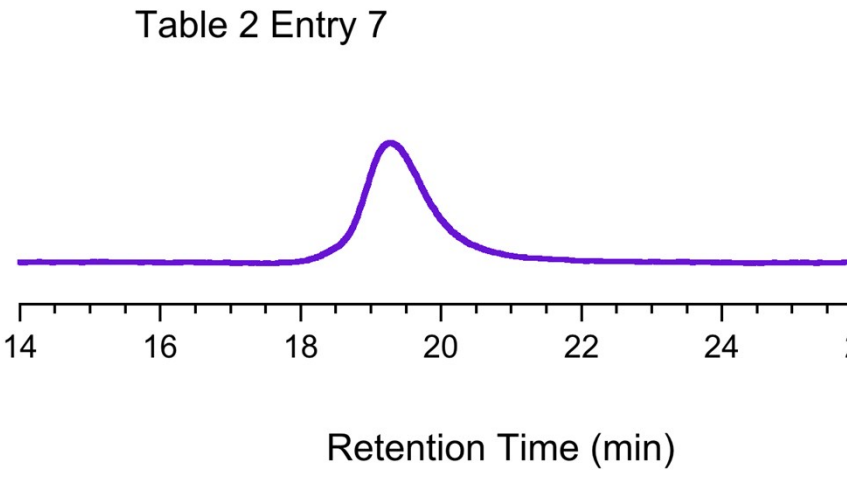

Figure S23. [1]H NMR and GPC trace of polymer from Table 2 Entry 7. *Toluene.

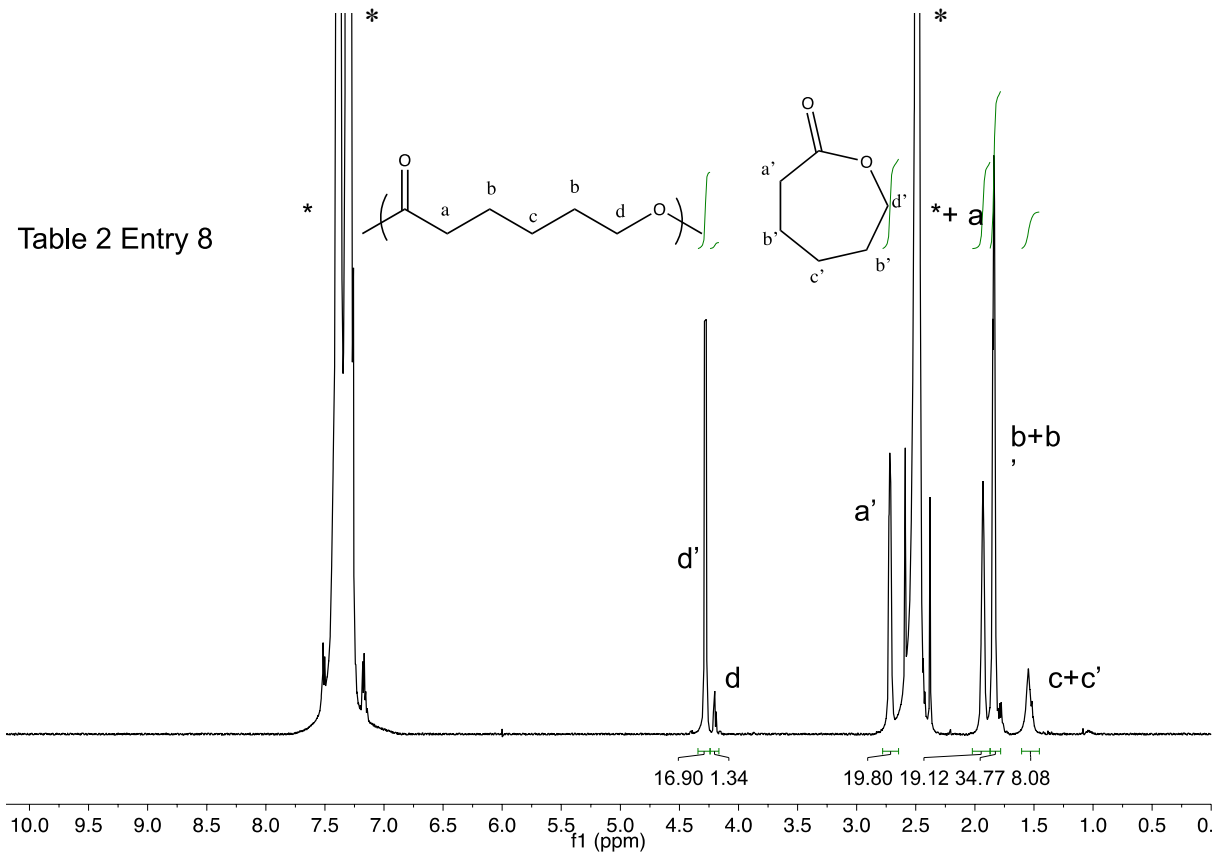

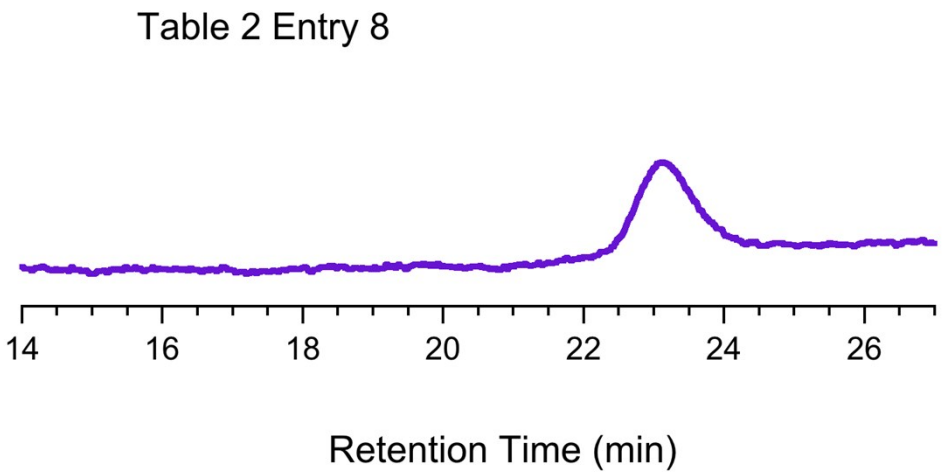

Figure S24. [1]H NMR and GPC trace of polymer from Table 2 Entry 8. *Toluene.

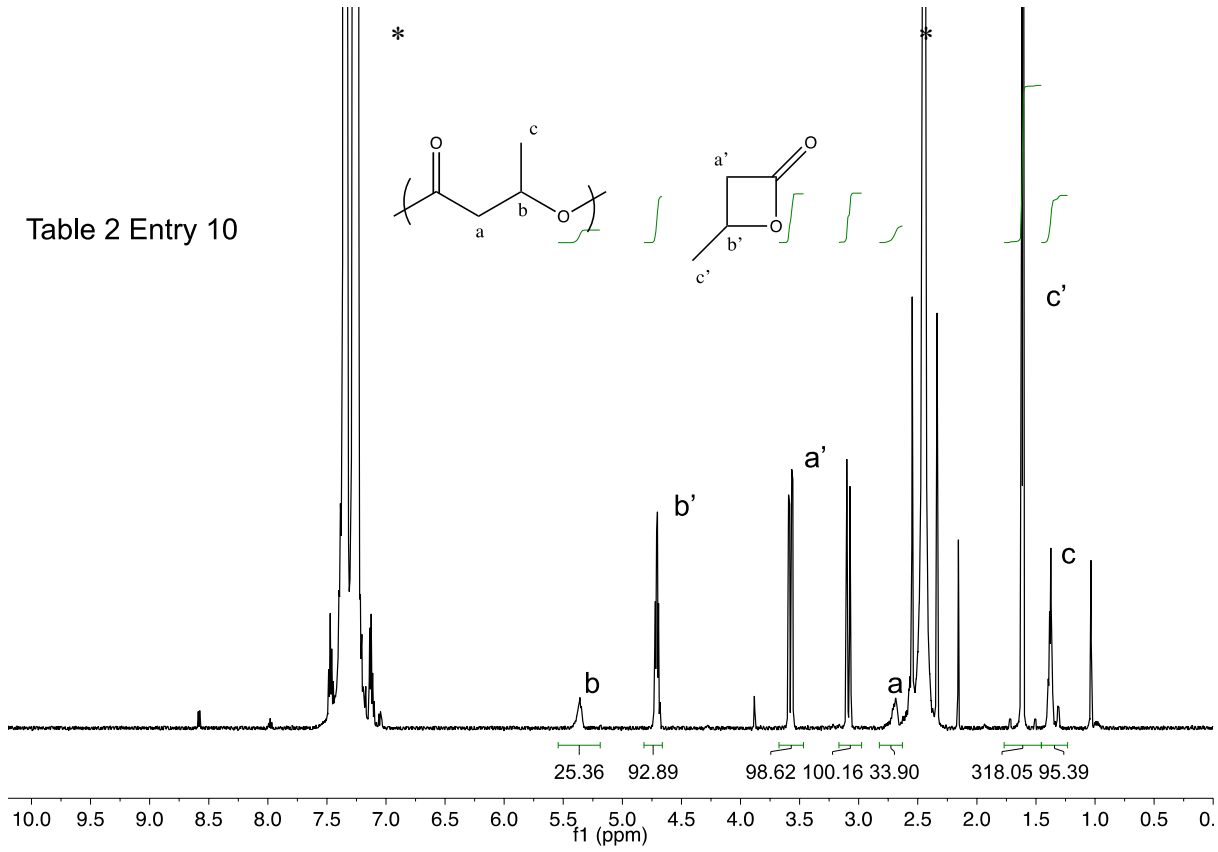

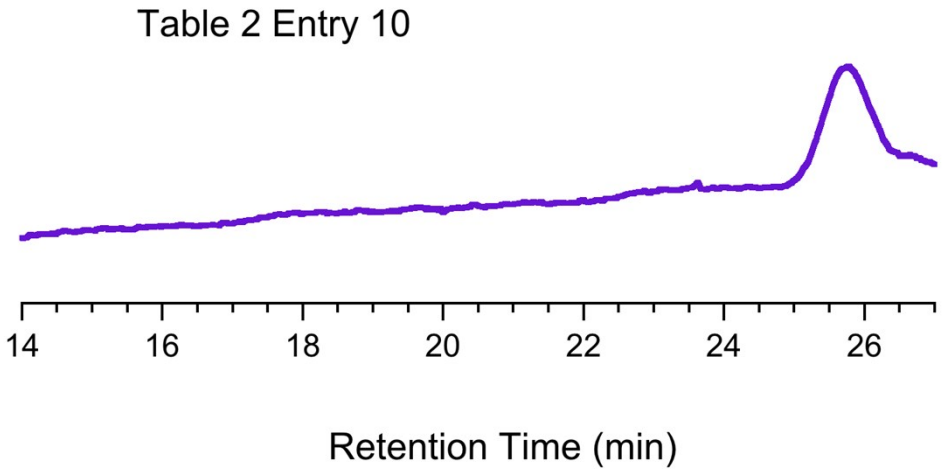

Figure S25. ^{1}H NMR and GPC trace of polymer from Table 2 Entry 10. *Toluene.

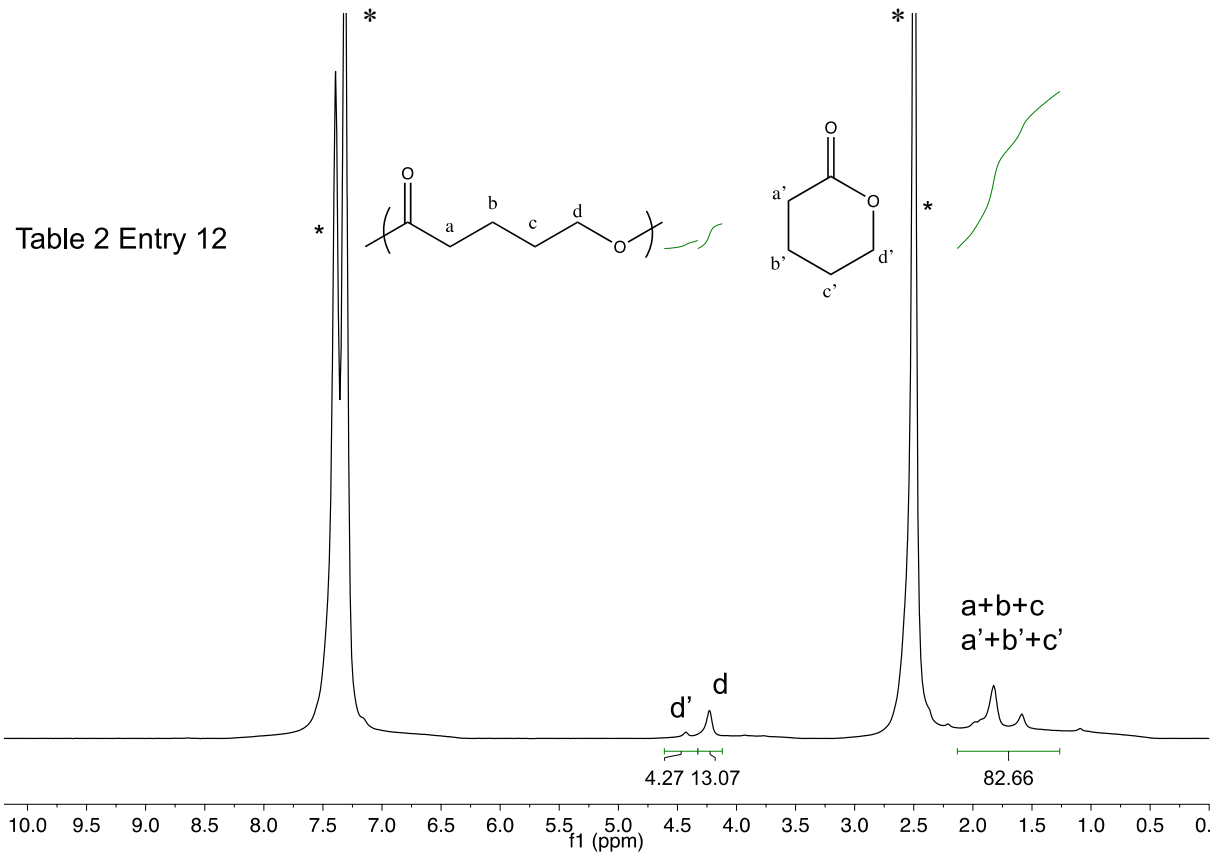

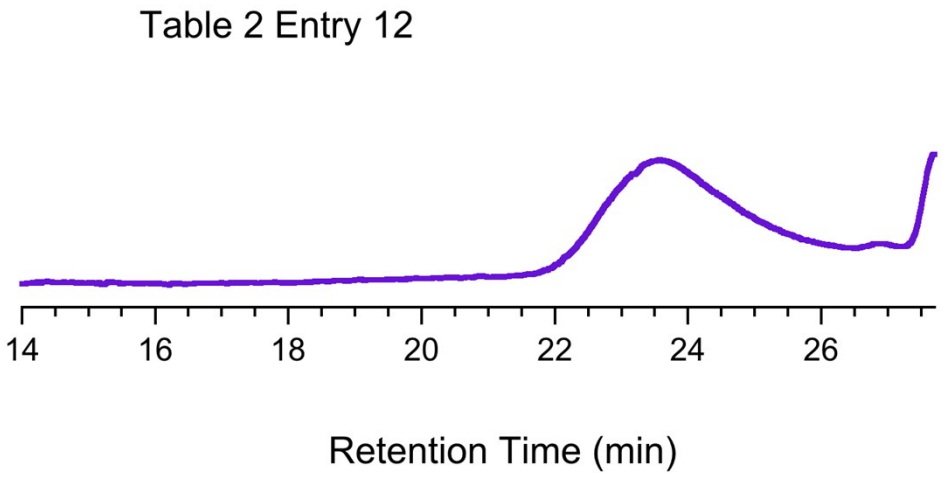

Figure S26. ^{1}H NMR and GPC trace of polymer from Table 2 Entry 12. *Toluene.

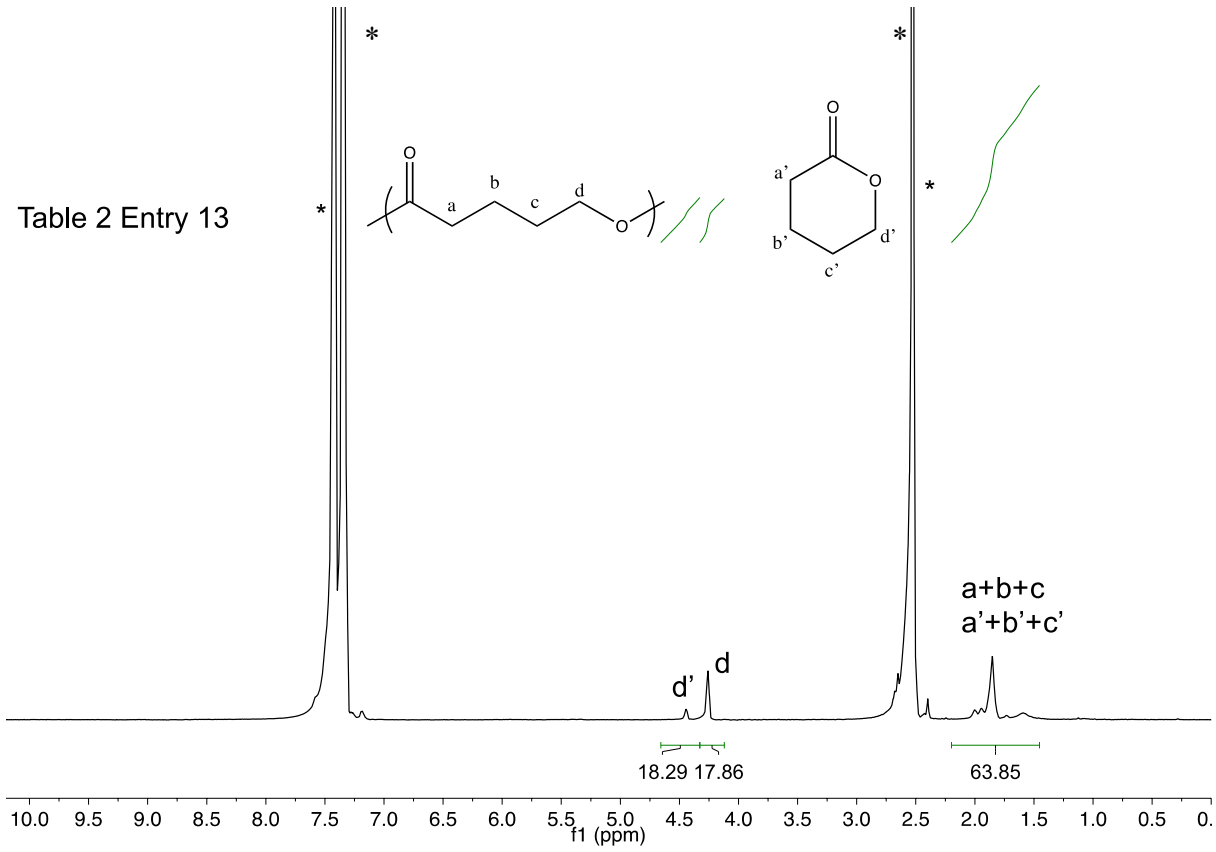

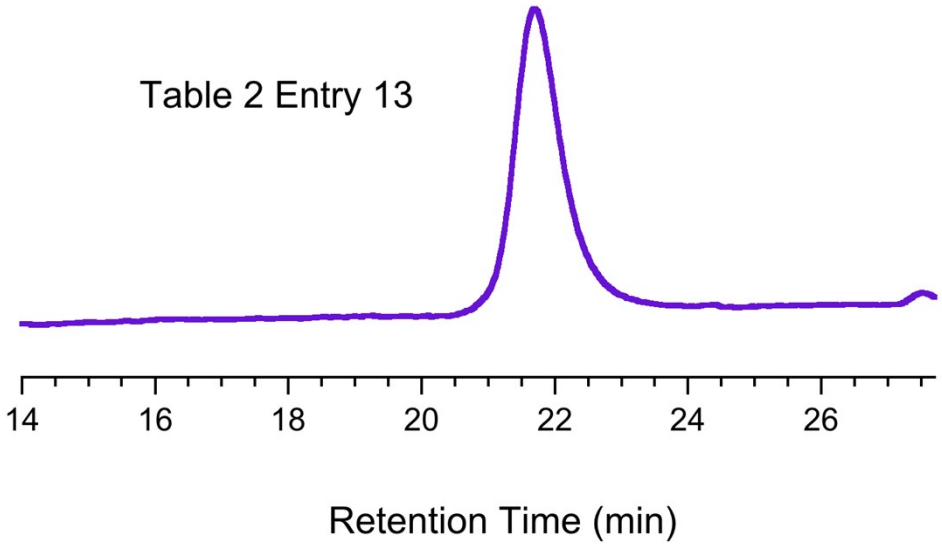

Figure S27. ^{1}H NMR and GPC trace of polymer from Table 2 Entry 13. *Toluene.

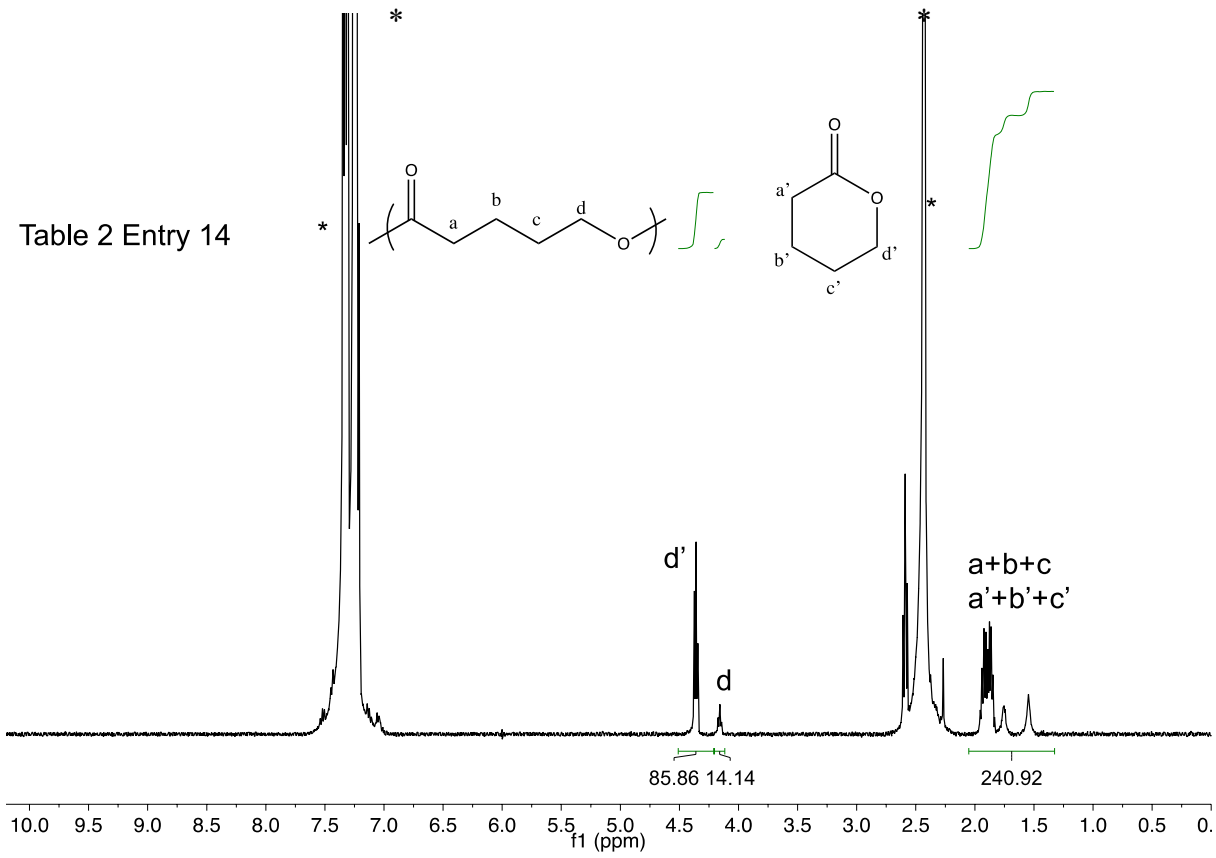

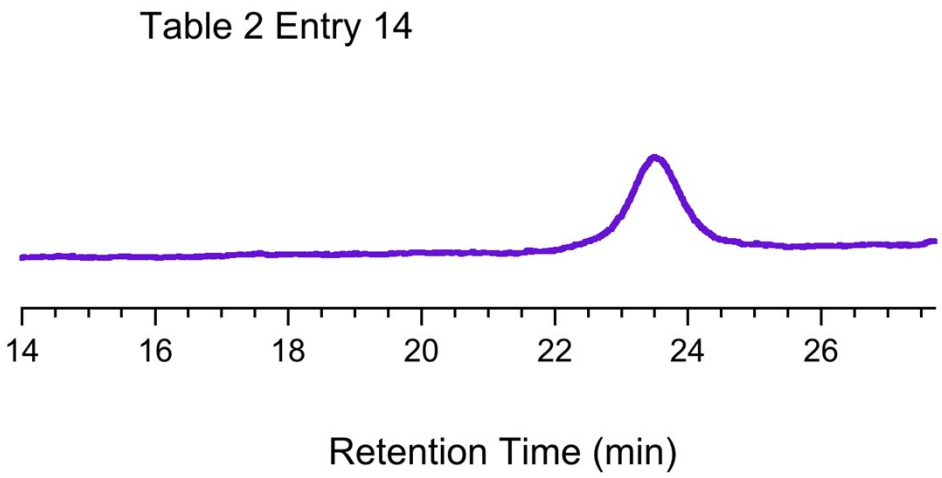

Figure S28. [1]H NMR and GPC trace of polymer from Table 2 Entry 14. *Toluene

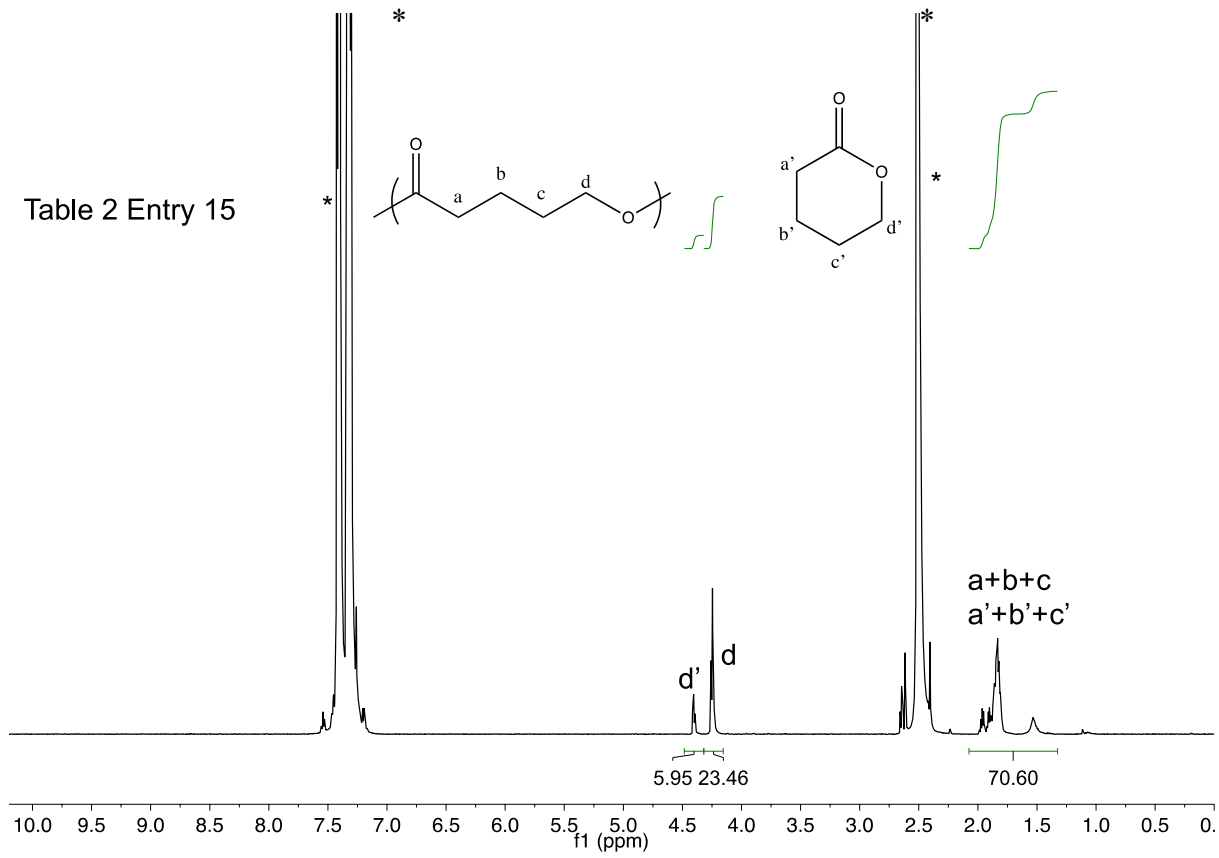

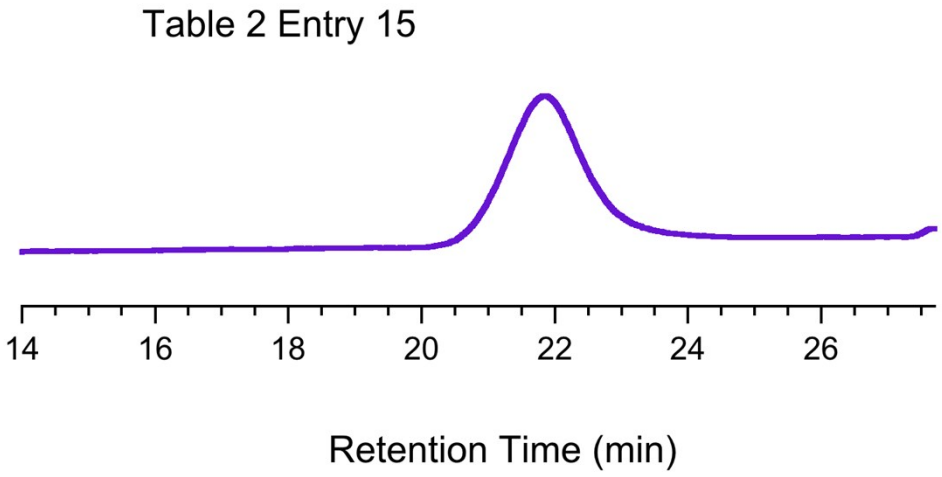

Figure S29. ^{1}H NMR and GPC trace of polymer from Table 2 Entry 15. *Toluene

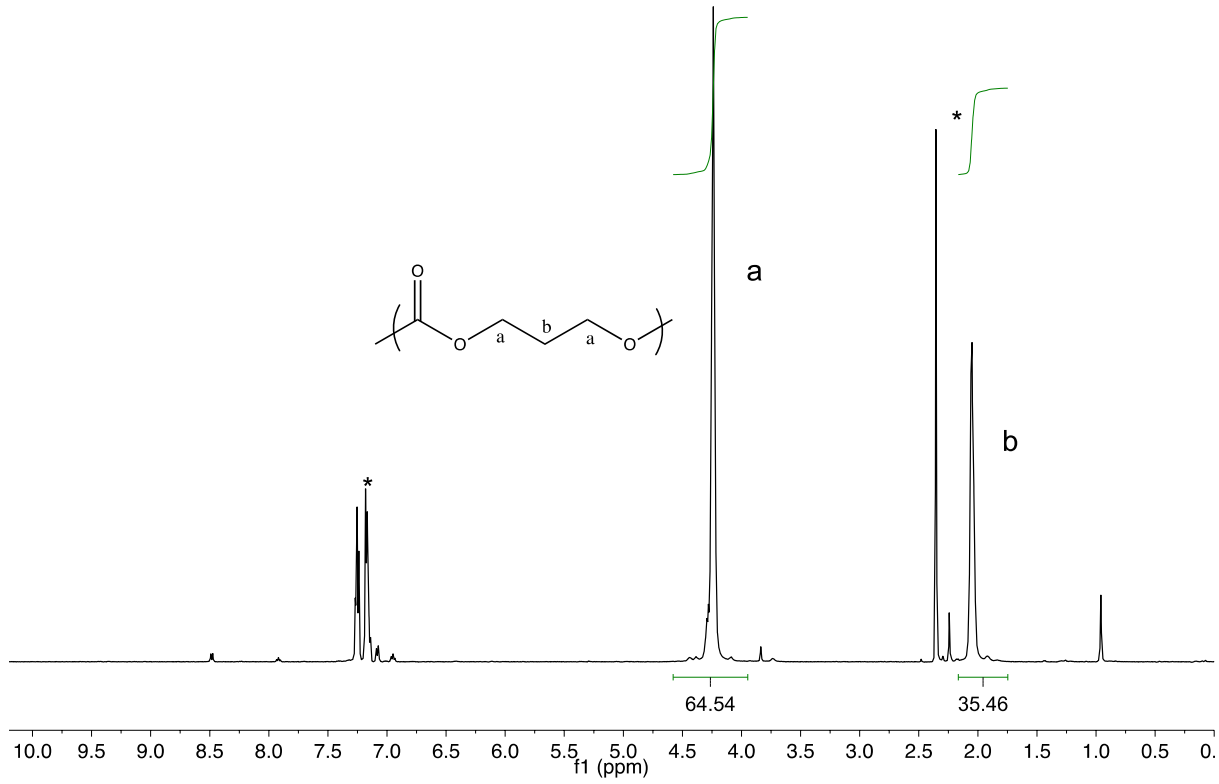

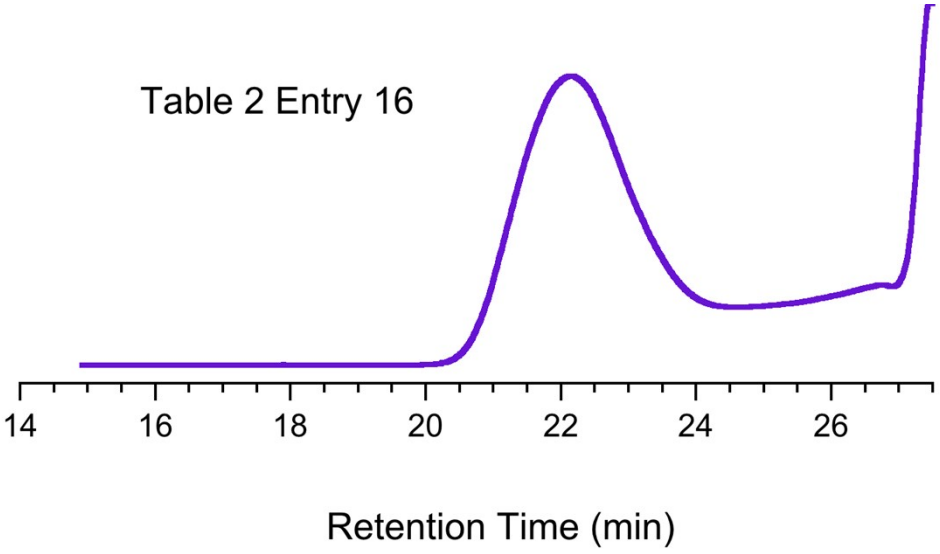

Figure S30. ^{1}H NMR and GPC trace of polymer from Table 2 Entry 16. *Toluene

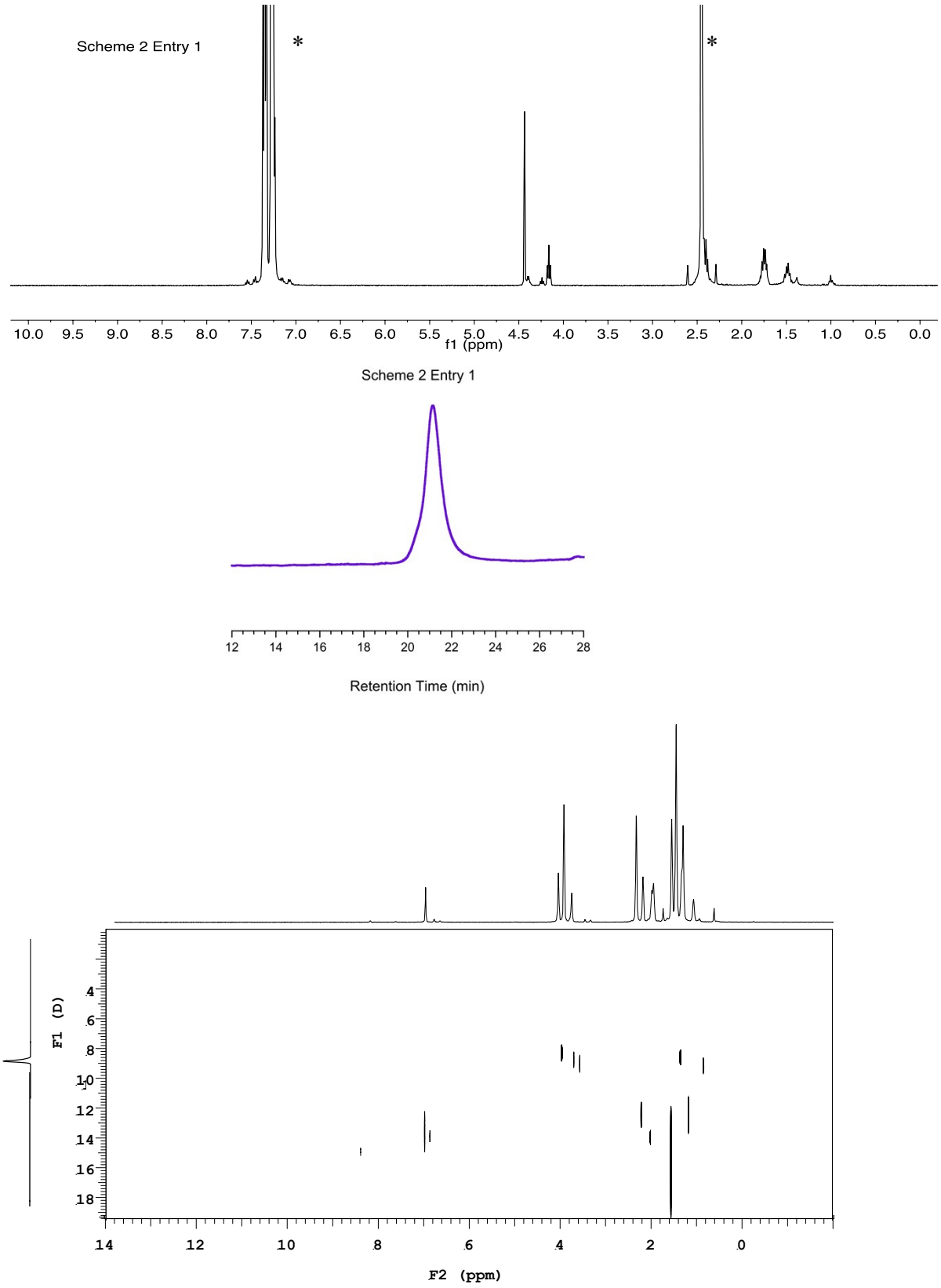

Figure S31. ^{1}H NMR, GPC trace, and DOSY of polymer from Scheme 2 Entry 1.

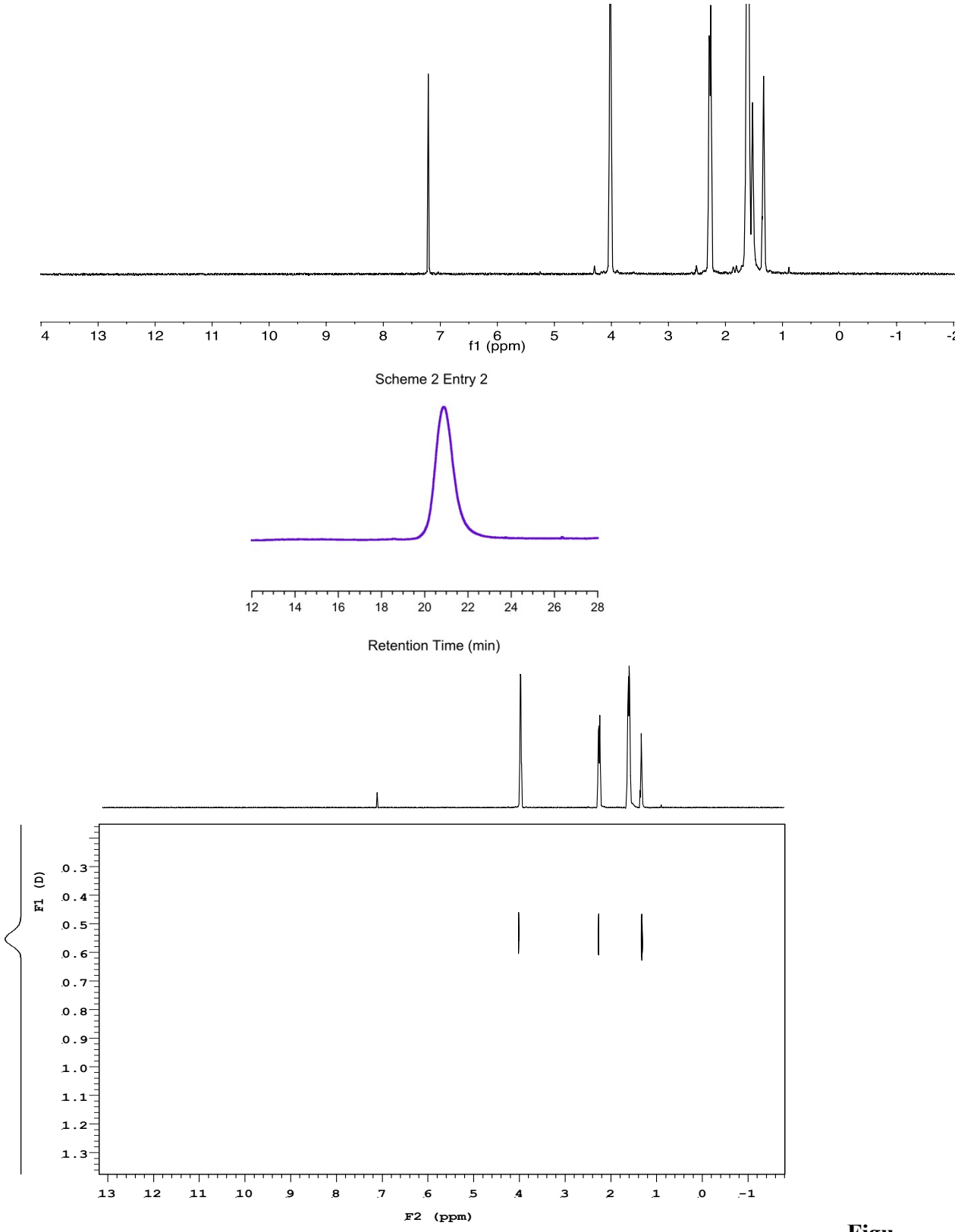

Figure S31. ^{1}H NMR, GPC trace, and DOSY of polymer from Scheme 2 Entry 2.

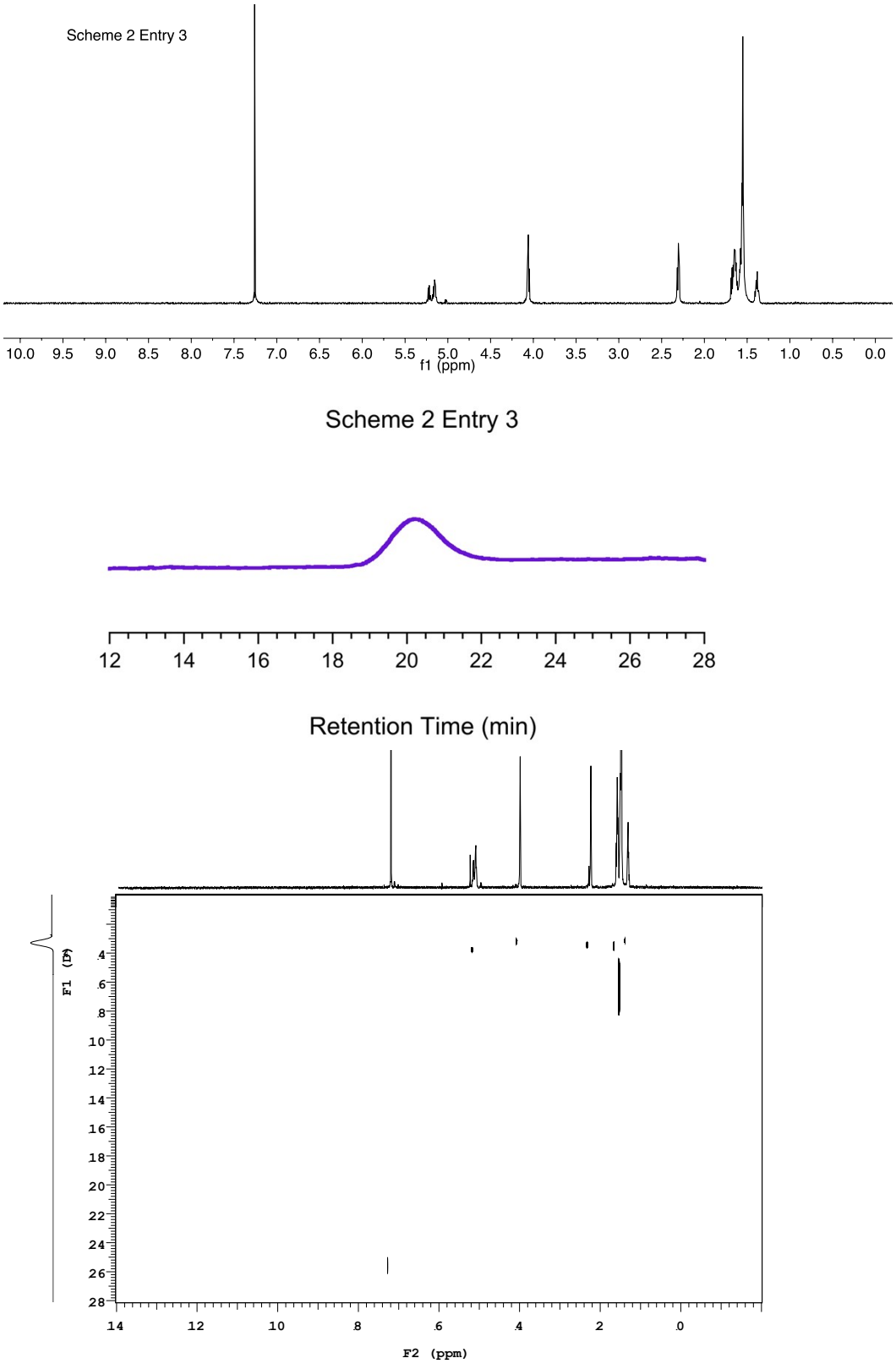

Figure S32. ^{1}H NMR, GPC trace, and DOSY of polymer from Scheme 2 Entry 3.

References

1. B. J. Burger and J. E. Bercaw, *New Developments in the Synthesis, Manipulation and Characterization of Organometallic Compounds*; A. L. Wayda and M. Y. Darensbourg, M.Y., Eds.; American Chemical Society: Washington D.C., 1987.
2. *(a)* D. F. Evans, *J. Chem. Soc.*, **1959**, 2003-2005; *(b)* E. M. Schubert, *J. Chem. Educ.*, 1992, **69**, 62.
3. G. J. P. Britovsek, V. C. Gibson, S. K. Spitzmesser, K. P. Tellmann, A. J. P. White and D. J. Williams, *J. Chem. Soc., Dalton Trans.*, 2002, 1159.
4. S. Stoll and A. Schweiger, *J. Magn. Reson.*, 2006, **178**, 42.
5. JulX: E. Bill, julX version 1.5, MPI for Chemical Energy Conversion, Germany, 2013
6. M. W. Bouwkamp, S. C. Bart, E. J. Hawrelak, R. J. Trovitch, E. Lobkovsky and P. J. Chirik, *Chem. Commun.*, 2005, 3406.
7. C. J. Cramer and D. G. Truhlar, *Phys. Chem. Chem. Phys.*, 2009, **11**, 10757.
8. M. J. Frisch et al. Gaussian 09, Revision E.01; Gaussian, Inc.: Wallingford, CT, 2016.
9. Y. Zhao and D. G. Truhlar, *J. Chem. Phys.*, 2006, **125**, 19410.
10. *(a)* Y. Zhao and D. G. Truhlar, *Acc. Chem. Res.*, 2008, **41**, 157; *(b)* Y. Zhao and D. G. Truhlar, *Chem. Phys. Lett.*, 2011, **502**, 1.
11. F. Weigend and R. Ahlrichs, *Phys. Chem. Chem. Phys.*, 2005, **7**, 3279.
12. *(a)* V. N. Staroverov, G. E. Scuseria, J. Tao and J. P. Perdew, *J. Chem. Phys.*, 2003, **119**, 12129; *(b)* J. Tao, J. P. Perdew, V. N. Staroverov and G. E. Scuseria, *Phys. Rev. Lett.*, 2003, **91**, 146401.
13. S. Grimme, J. Antony, S. Ehrlich and H. Krieg, *J. Chem. Phys.*, 2010, **132**, 154104.
14. *(a)* S. Grimme, S. Ehrlich and L. Goerigk, *J. Comp. Chem.*, 2011, **32**, 1456; *(b)* L. Goerigkab and S. Grimme, *Phys. Chem. Chem. Phys.*, 2011, **13** 6670.
15. A. D. Boese and N. C. Handy, *J. Chem. Phys.*, 2002, **116**, 9559.
16. *(a)* A. D. Becke, *J. Chem. Phys.*, 1993, **98**, 5648; *(b)* C. Lee, W. Yang and R. G. Parr, *Phys. Rev. B: Condens. Matter Mater. Phys.*, 1988, **37**, 785; *(c)* P. Stephens, F. J. Devlin, C. F. Chabalowski and M. J. Frisch, *J. Phys. Chem.*, 1994, **98**, 11623.
17. H. S. Yu, X. He, S. L. Li and D. G. Truhlar, *Chem. Sci.*, 2016, **7**, 5032.
18. A. D. Becke, *J. Chem. Phys.*, 1997, **107**, 8554.
19. *(a)* J. P. Perdew, K. Burke and M. Ernzerhof, *Phys. Rev. Lett.*, 1996, **77**, 3865; *(b)* J. P. Perdew, K. Burke and M. Ernzerhof, *Phys. Rev. Lett.*, 1997, **78**, 1396.
20. *(a)* N. C. Handy and A. J. Cohen, *Mol. Phys.*, 2001, **99**, 403; *(b)* W.-M. Hoe, A. Cohen and N. C. Handy, *Chem. Phys. Lett.*, 2001, **341**, 319.
21. P. Milko, M. A. Iron, *J. Chem. Theory Comput.*, 2014, **10**, 220.
22. *(a)* M. Swart, *J. Chem. Theory Comput.*, 2008, **4**, 2057; *(b)* M. Swart, *Chem. Phys. Lett.*, 2013, **580**, 166; *(c)* P. Verma, Z. Varga, J. E. M. N. Klein, C. J. Cramer, L. Que Jr. and D. G. Truhlar, *Phys. Chem. Chem. Phys.*, 2017, DOI: 10.1039/c7cp01263b

23. *(a)* K. Yamaguchi, F. Jensen, A. Dorigo and K. N. Houk, *Chem. Phys. Lett.*, 1988, **149**, 537; *(b)* T. Soda, Y. Kitagawa, T. Onishi, Y. Takano, Y. Shigeta, H. Nagao, Y. Yoshioka and K. Yamaguchi, *Chem. Phys. Lett.*, 2000, **319**, 223.
24. *(a)* F. Neese, *Inorg. Chim. Acta*, 2002, **337**, 181; *(b)* S. Sinnecker, L. D. Slep, E. Bill and F. Neese, *Inorg. Chem.*, 2005, **44**, 2245.
25. M. Römelt, S. Ye and F. Neese, *Inorg. Chem.*, 2009, **48**, 784.
26. A. M. Tondreau, S. C. E. Stieber, C. Milsmann, E. Lobkovsky, T. Weyhermüller, S. P. Semproni and P. J. Chirik, *Inorg. Chem.*, 2013, **52**, 635.
27. H. Zhang, Z. Ouyang, Y. Liu, Q. Zhang, L. Wang and L. Deng, *Angew. Chem. Int. Ed.*, 2014, **53**, 8432.
28. F. Neese, *WIREs Comput. Mol. Sci.*, 2012, **2**, 73.
29. D. Rappoport and F. Furche, *J. Chem. Phys.*, 2010, **133**, 134105.
30. A. Klamt and G. Schüürmann, *J. Chem: Soc., Perkin. Trans. 2,* 1993, **5**, 799.
31. A. V. Marenich, C. J. Cramer and D. G. Truhlar, *J. Phys. Chem. B*, 2009, **113**, 6378.